PERGAMON

Atmospheric Environment 34 (2000) 1323–1354

ATMOSPHERIC ENVIRONMENT

www.elsevier.com/locate/atmosenv

The influence of stratospheric intrusions on alpine ozone concentrations

A. Stohl[a,*], N. Spichtinger-Rakowsky[a], P. Bonasoni[b], H. Feldmann[c], M. Memmesheimer[c], H.E. Scheel[d], T. Trickl[d], S. Hübener[e], W. Ringer[f], M. Mandl[g]

[a]*Lehrstuhl für Bioklimatologie und Immissionsforschung, Ludwig-Maximilians-Universität München, Am Hochanger 13, D-85354 Freising-Weihenstephan, Germany*

[b]*Istituto per lo Studio dei Fenomeni Fisici e Chimici della Bassa ed Alta Atmosfera, Consiglio Nazionale delle Ricerche, Via Gobetti 101, I-40129 Bologna, Italy*

[c]*Institut für Geophysik und Meteorologie, Universität zu Köln, Aachener Straße 201-209, D-50931 Köln, Germany*

[d]*Fraunhofer-Institut für Atmosphärische Umweltforschung (IFU), Kreuzeckbahnstr. 19, D-82467 Garmisch-Partenkirchen, Germany*

[e]*Laboratorium für Radio- und Umweltchemie, Departement für Chemie und Biochemie, Universität Bern, Freiestrasse 3, CH-3012 Bern, Switzerland*

[f]*Bundesanstalt für Lebensmitteluntersuchung, Derfflingerstraße 2, A-4017 Linz, Austria*

[g]*Zentralanstalt für Meteorologie und Geodynamik, Freisaalweg 16, A-5020 Salzburg, Austria*

Received 25 January 1999; received in revised form 22 June 1999; accepted 13 July 1999

Abstract

This paper presents studies of stratospheric intrusions in the Alps and northern Apennines, their seasonal variations, and their effect on ozone concentrations. The results are based on experimental data and on simulations with a Lagrangian tracer model. The model, employing analyzed meteorological data, advects a passive stratospheric ozone tracer through the calculation of a large number of three-dimensional trajectories. In two case studies, the model is evaluated using a comprehensive set of observation data, consisting of water vapor satellite images, total column ozone measurements, ozone soundings, and measurements of ozone, beryllium 7 and meteorological parameters at three high Alpine sites and at the highest peak in the northern Apennines. During the two episodes considered, stratospheric air was detectable in the whole Alpine area with peak ozone mixing ratios in the 70–90 ppb range and even penetrated into some valleys. During one episode, stratospheric air also reached the northern Apennines, which highlights the large extension of the affected region. At the end of this episode, as shown by the model, the air was a mixture of tropospheric air with air originating from three different stratospheric intrusions. For three high Alpine sites, the frequency of stratospheric intrusions and its seasonal variation is derived using ozone, beryllium 7 and humidity measurements. The periods covered by this climatology are 1991 to 1997 for Zugspitze, and 1996 to 1998 for Jungfraujoch and Sonnblick. Another short climatology was established from a three-year (1995–1997) model simulation. Good agreement between the two approaches is found for Zugspitze and Sonnblick: the simulated ozone tracer mixing ratios are significantly higher on "intrusion days", identified from the observations, than on "non-intrusion days". For Jungfraujoch, the agreement is less good, which could partly be due to the coarser time resolution of the beryllium 7 measurements at this site. The absolute frequency of stratospheric air intrusions as identified from the observations depends critically on the specification of threshold values for ozone, beryllium 7 and humidity, while the relative shape of the annual cycle is rather insensitive to threshold variations. At Zugspitze and Sonnblick, it shows a maximum in October, a secondary maximum in January and February, and a deep summer minimum. For Jungfraujoch, where the frequency of intrusions is higher than at Zugspitze and Sonnblick throughout most of the year, no clear seasonal variation is found. Simulated ozone tracer mixing ratios in the Alps are found to peak in late-winter/early-spring, when ozone concentrations are at a maximum in the stratosphere, but are almost at the same level in autumn, due to somewhat higher frequency of stratospheric

* Corresponding author. Fax: + 49-8161-71-4753.

1352-2310/00/$ - see front matter
PII: S1352-2310(99)00320-9

intrusions in that season. Similar to the observations, there is a deep minimum in summer, when the model showed practically no intrusions with a tropospheric age of less than four days.

Keywords: Stratospheric intrusions; Ozone; Beryllium 7; Alps; Lagrangian model

1. Introduction

Tropospheric ozone (O_3) is photochemically produced in situ, but it is also transported down from the stratosphere. The relative importance of these two sources for its budget, both globally (e.g., Roelofs and Lelieveld, 1997) and regionally (e.g., Mauzerall et al., 1996), is still poorly understood. Viewed from a global perspective and on long time scales, there is an organized upwelling from the troposphere to the stratosphere in the tropics (Plumb, 1996; Mote et al., 1996), isentropic transport to the extratropics in the stratosphere (Waugh, 1996), and a downward mass flux from the stratosphere to the troposphere in middle and higher latitudes (Holton et al., 1995). According to the downward control principle (Haynes et al., 1991), mass transfer from higher levels of the stratosphere to the troposphere at midlatitudes is largely controlled non-locally by dynamical processes responsible for the global-scale mean circulation in the middle atmosphere. It can be used to estimate the overall flux of air across a control surface in the stratosphere which, in combination with variations in tropopause height, explains the often observed spring-time maximum of stratospheric tracer concentrations in the troposphere (Appenzeller et al., 1996b).

The downward control principle is less suitable for determining the exchange between the lower stratosphere and the troposphere (Chen, 1995), since this is highly episodic, can occur in both directions and is caused by several different mechanisms. Stratosphere to troposphere exchange in tropopause folds (Danielsen, 1968; Vaughan, 1988; Ebel et al., 1991; Lamarque and Hess, 1994; Vaughan et al., 1994; Beekmann et al., 1997), cut-off lows (Vaughan, 1988; Ebel et al., 1991; Ancellet et al., 1994), in mesoscale convective complexes (Poulida et al., 1996) and thunderstorms (Tremblay and Servranckx, 1993), and due to breaking gravity waves (Lamarque et al., 1996) have received attention. Exchanges in tropopause folds and in cut-off lows are most important.

Intruding stratospheric air may contribute significantly to the tropospheric background O_3 concentrations (Fabian and Pruchniewicz, 1977) because of the long chemical lifetime (order of one to two months) of O_3 in the free troposphere (Fishman et al., 1979; Liu et al., 1987). During pre-industrial times, when surface O_3 concentrations were much lower than today (Volz and Kley, 1988), stratospheric intrusions were their major source, but their exact contribution to the present tropospheric O_3 budget is debated. Uncertainties arise from the differences between existing estimates of the amount of O_3 transferred across the tropopause, and also from uncertainties in the further fate, both physical and chemical, of stratospheric O_3 in the troposphere.

Attempts to quantify the stratosphere–troposphere exchange (STE) of O_3 were based on observations as well as on model calculations. One widespread method to diagnose the air flux across the tropopause is the application of Wei's formula (Wei, 1987; Lamarque and Hess, 1994), although Wirth (1995) and Wirth and Egger (1999) found this to be rather inaccurate. Often, exchange rates obtained for a few cases have been upscaled with the detected frequency of tropopause folds. In this way, Beekmann et al. (1997) recently estimated the northern hemispheric O_3 flux across the tropopause due to tropopause folds alone to be 5.7 (4.4–7.0) $\times 10^{10}$ mol cm^{-2} s^{-1}, a figure in agreement with older model studies (Levy et al., 1985; Ebel et al., 1991), whereas Murphy and Fahey (1994), using a different method, arrived at only 3.5 (1.5–6.8) $\times 10^{10}$ mol O_3 cm^{-2} s^{-1} for the total STE.

Once brought into the troposphere, the stratospheric air is quasi-adiabatically stirred by the large-scale cyclonic and anticyclonic disturbances (Mahlmann, 1997) and often develops elongated, slender streamers that break up into trains of vortices (Appenzeller and Davies, 1992). Because of this, the characteristic signature of stratospheric air (high O_3 content, low humidity, etc.) gets lost over the period of a few days. If fragmentation and mixing with the surrounding tropospheric air is not already completed on the way down through the free troposphere, these delicate structures are rapidly destroyed when getting entrained into the planetary boundary layer. This makes it very difficult to observe stratospheric intrusions in the lower troposphere and especially at the surface. Only the most vigorous events produce spikes in measured stratospheric tracer concentrations that are distinct enough to draw the attention of the analyst to a possible stratospheric influence. Furthermore, there is hardly a tracer of stratospheric air which allows a quantitative analysis of stratospheric intrusions. Probably because of these difficulties, some observational studies come to the conclusion that on average there is no large contribution of stratospheric O_3 at the surface (e.g., Dibb et al., 1994; Derwent et al., 1998). In other observational studies, however, a much larger impact of stratospheric O_3 at the surface was found (e.g., Parrish et al., 1998) and numerous individual stratospheric intrusion events associated with elevated surface

O_3 concentrations are documented in the literature (e.g., Wakamatsu et al., 1989; Lisac et al., 1993; Tremblay and Servranckx, 1993; Davies and Schuepbach, 1994). The discrepancy between the above studies may be explained by the fact that in the measurement data only intrusions descending directly from the stratosphere can be detected. More indirectly intruding stratospheric air, which travels horizontally or even ascends over some period, has time to mix strongly with surrounding tropospheric air, thereby loosing its stratospheric characteristics.

Also modeling studies come to different results concerning the relative contribution of stratospheric intrusions to the tropospheric O_3 budget. Roelofs and Lelieveld (1997) performed calculations with a coupled chemistry-general circulation model and found that approximately 40% of the O_3 in the troposphere is of stratospheric origin. In a study using backward trajectories to two locations in the Canadian arctic, Bachmeier et al. (1994) estimated that 80% of the five-day backward trajectories terminating in the upper troposphere, and 40% of the trajectories terminating in the middle troposphere experienced "stratospheric input". Austin and Follows (1991) and Follows and Austin (1992), on the other hand, concluded that stratospheric O_3 contributes only 25% at 300 hPa and less than 5% at the surface.

At least for mountain summits a frequent stratospheric influence is generally agreed upon (Reiter et al., 1983; Reiter, 1991). This is mostly due simply to their altitude (e.g. Tsutsumi et al., 1998), but partly also to the frequency of lee cyclogenesis, caused by the mountain ranges themselves (Buzzi et al., 1984). This encouraged us to include the study of these phenomena into the VOTALP (Vertical Ozone Transports in the Alps) project, which studied photochemical and transport processes relevant to the ozone level in the Alps and Northern Apennines. During VOTALP, Eisele et al. (1999) compared descending ozone-rich structures in lidar data and found that most of them reached a level of 3000 m. Scheel et al. (1999) used different criteria to detect stratospheric intrusions from measurement data at the Zugspitze. They found a strong stratospheric influence during 5–6% of the time, and a weaker, but still clear influence during more than 10% of the time. However, they noted that "the overall statistics are critically dependent on the applied criteria for the threshold levels". Elbern et al. (1997) found that in a ten-year period direct deep intrusions of stratospheric air could be identified from records of beryllium 7 (^{7}Be), O_3 and humidity at the Zugspitze peak (2962 m asl) during 5% of the time. At the neighboring, but lower, Wank summit (1776 m asl) less than half of these events were found, while at the valley floor in Garmisch-Partenkirchen (740 m) none of them produced resolvable signatures. Reiter (1991), by analyzing measurement data obtained aboard the Zugspitze cable car, also concluded that stratospheric intrusions do not penetrate to heights lower than 1600 m asl. In all of the above studies, because of the mixing with tropospheric air, it was not known what fraction of the O_3 present during stratospheric intrusions actually came from the stratosphere. Furthermore, strongly diluted stratospheric air escaped detection in these studies. Thus, the relative contribution of stratospheric O_3 to the O_3 level at mountain peaks is still unknown.

In this paper, we examine how strongly stratospheric intrusions influence O_3 concentrations at alpine peaks by using both measurement data and model calculations. For a map of the investigation area and the site locations see Fig. 1. The structure of the paper is as follows: First, we introduce the model used to simulate stratospheric intrusions (Section 2). Then, we briefly describe the available observations (Section 3). Using these data, the model is evaluated in two case studies (Section 4). Next, we present two short climatologies of stratospheric intrusions: one derived from the measurements (Section 5), the other based on a three-year model simulation (Section 6). Finally, in Section 7, the results are discussed.

2. The tracer transport model

For our investigations we used a special version of the stochastic Lagrangian particle model FLEXPART (based on version 3.0). FLEXPART evolved from the trajectory model FLEXTRA (Stohl et al., 1995; Baumann and Stohl, 1997; Stohl and Seibert, 1998) and is normally used to calculate the dispersion from point sources (Stohl, 1998a). It was extensively evaluated by Stohl et al. (1998) with large-scale tracer experiment data. FLEXPART represents transport and dispersion by calculating the three-dimensional trajectories of a multitude of particles. This Lagrangian (as opposed to the Eulerian) concept has several attractive features. For this study, the two most important advantages over Eulerian models are: first, the transport is more accurately described because there are no numerical inaccuracies due to the advection scheme (which is especially important in regions with large spatial concentration gradients, as near tropopause folds); second, individual particles move independently from each other and can thus carry additional information. We mark them with the time they cross the tropopause, since this gives information on the time the tracer has travelled in the troposphere (furtheron referred to as its age). If multiple intrusions contribute to the tracer concentrations at the same time and location, the age also allows to separate their relative contributions. Note that the approach adopted here is different from contour advection, another Lagrangian technique (e.g., Norton, 1994; Waugh and Plumb, 1994). With contour advection, the aim is to achieve very high resolution to study fine-scale structures. However, contour advection is two-dimensional (isentropic), and mixing is not explicitly simulated.

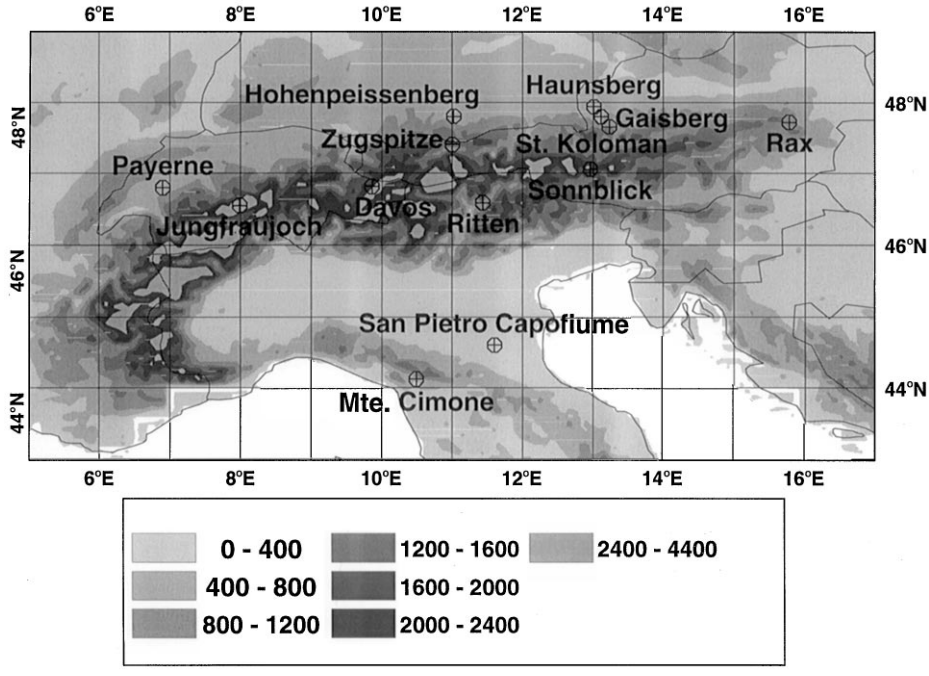

Fig. 1. Topography of the Alpine region (m asl) and locations of the measurement sites.

FLEXPART is based on data of the T213 L31 numerical weather prediction model of the European Centre for Medium-Range Weather Forecasts (ECMWF, 1995). We used data from the lowest 29 model levels with a horizontal resolution of 1° and a time resolution of 3 h (analyses at 0, 6, 12, 18 UTC; 3 h forecasts at 3, 9, 15, 21 UTC). The model domain stretched from 50°W to 50°E and from 25°N to 80°N. This is sufficiently large for simulating the intrusions discussed in the case studies, but it is an important constraint for the three-year simulation, since intrusions occurring outside this domain are missing in the resulting climatology. To obtain a rough indication of the validity of our simulations in this respect, we calculated backward trajectories during our investigation period arriving every 3 h at the four high mountain sites. Depending on the station, 71–86% (55–74%) of the trajectories originating in the stratosphere extended at least 4 (5) days backward in time before encountering the domain boundary. Therefore, our climatology will strongly underestimate the influence of older stratospheric intrusions. However, it adequately covers direct intrusions which are most likely to produce clear signatures in the measurements.

The input data used for our model calculations need some critical discussion. First, the Alpine topography is not well resolved by the ECMWF model and dynamic effects induced by the Alps, such as foehn flow, gravity waves, or lee cyclogenesis, are not fully captured. Small-scale processes, such as slope winds, are almost completely missing in the simulations, which most strongly affects the model results for the lowest levels in the Alpine region. Second, although many authors have shown the suitability of ECMWF data – even at lower resolution than used here – to study stratospheric intrusions (e.g., Chen, 1995; Appenzeller et al., 1996a; van Velthoven and Kelder, 1996), small-scale structures of the intrusions are poorly resolved. Third, the ECMWF data used are a sequence of initialized analyses. Although each meteorological field is the best possible estimate of the true conditions at its validation time, they are not dynamically consistent with each other. Stohl and Seibert (1998) showed that these inconsistencies impair the accuracy of trajectory calculations.

The adequate representation of the large-scale motions, including the vertical wind component, is crucial. One might expect that errors in the interpolation of the wind velocity are larger in tropopause folds than outside and trajectory calculations hence less accurate, but according to Scheele et al. (1996) this is not the case. Stohl and Seibert (1998) demonstrated that the accuracy of the vertical wind in the ECMWF data is very high and that three-dimensional trajectories calculated from these data are clearly more accurate than isentropic trajectories. For a discussion on trajectory errors see Stohl (1998b).

For particles in the planetary boundary layer, FLEXPART solves Langevin equations for the three wind velocity components (Thomson, 1987), assuming that the particle positions and velocities evolve as a Markov

process. Gaussian turbulence is assumed under all meteorological conditions, and the turbulent statistics are obtained using the scheme of Hanna (1982) with some modifications for convective conditions. A density correction (Stohl and Thomson, 1999) is applied to account for the decrease of density with height.

Uncertainties arise from the fact that not all vertical transport processes are adequately treated in the model. Deep convection overshooting the local tropopause may transfer stratospheric O_3 from higher levels to the surface. Its neglect in the model causes an unknown underestimation of the stratospheric O_3 transferred to the lower troposphere in the model, although currently there is no evidence for a large contribution of this process on a seasonal basis. Turbulence in the free troposphere is assumed to be proportional to the horizontal and vertical wind shear. This parameterization is not adequate for regions with strong turbulence as, for instance, near jet streaks. The uncertainty and its direction caused by the lack of a more realistic turbulence parameterization is unknown.

We use FLEXPART to simulate the transport of two tracers that are both initialized only in the stratosphere. The first tracer simply represents stratospheric air; the second one represents O_3. For this purpose, the whole model domain up to 15 km above the ground is divided into boxes, and each particle initially represents a volume of 30 km × 30 km × 134 m. Whether a particle is stratospheric or not is determined using the dynamical definition of the tropopause based on a threshold value for the potential vorticity (PV). Threshold values reported in the literature range from 1.0 potential vorticity units (pvu, 1 pvu $= 1 \times 10^{-6}$ m^2 K kg^{-1} s^{-1}) (Danielsen, 1968) to 3.5 pvu (Hoerling et al., 1991). Partly, this value depends on the vertical resolution of the meteorological data, and partly it depends on the synoptic situation and the geographical location (Hoinka, 1997). We used the rather low value of 1.6 pvu, since the vertical resolution of the ECMWF model level data is higher than that of the mandatory pressure-level data used in many other studies (for instance, Hoerling et al., 1991). Furthermore, Bethan et al. (1996) found that the "ozone tropopause" is on average almost 1000 m lower than the "thermal tropopause". Since our main focus is on O_3, our choice of the tropopause definition seems appropriate. A sensitivity study of a three-month period showed that increasing the PV threshold to 2.5 pvu decreased the average O_3 tracer mixing ratios at the mountain peaks by 20–30%.

The mass of each stratospheric air tracer particle (tropospheric ones are dropped from the calculation) is obtained by multiplying the local air density with the volume a particle represents at the beginning. This procedure leads to a spatially uniform initial distribution of stratospheric particles, but particles at greater heights (where the density is lower) carry less mass than particles at lower heights. If air moves downwards, it is compressed and the volume a particle represents shrinks in the absence of dilution. Tracer mixing ratios are evaluated on a three-dimensional grid with a horizontal resolution of $1^\circ \times 1^\circ$, and a vertical resolution of 500 m below 4000 m asl and 1000 m above. 3-h mean values are calculated from samples taken every 15 min.

Particle trajectories are terminated at the outflowing boundary. At the inflowing boundary, the mass flux of air into the model domain is calculated. At each model time step (300 s), inflowing mass is accumulated, and when it exceeds a threshold value, consistent with the initialization procedure, a new particle is created. Typically, one to two million particles are tracked.

O_3 is represented by a passive ozone-like tracer in the model that does not undergo chemical reactions. The average photochemical lifetime of O_3 in the background free troposphere is of the order of one to two months (Fishman et al., 1979; Liu et al., 1987). Therefore, photolysis and chemical destruction, which are not included in the model, may diminish the stratospheric O_3 concentrations in the troposphere by a few percent up to some 20% on the time scales considered in this paper. Dry deposition of the O_3 tracer is determined using a resistance parameterization (Wesely, 1989).

The O_3 tracer is initialized in the stratosphere (above 1.6 pvu) using the relation O_3 (ppb) $= S$ (ppb pvu^{-1}) × PV (pvu) (Danielsen, 1968; Beekmann et al., 1994). To determine S, we used data from 526 ozone soundings during the period 1995 to 1997 at Hohenpeißenberg (11.0°E, 47.8°N), Payerne (6.9°E, 46.8°N) and San Pietro Capofiume (11.6°E, 44.6°N) at heights below 15 km (i.e., below the top of the model domain), but above the tropopause, interpolated PV from the model grid to the positions of the ozone sondes, and applied regression analysis. Correlation coefficients were mostly between 0.75 and 0.85.

A strong seasonal variation of S with a maximum in early spring and a minimum in fall was found at all stations. There was relatively small scatter in S between the three stations for a given month, which suggests that the average S used for model initialization is valid within 20%. Deviations of individual data points from this relationship, however, were often quite large, and may in some cases lead to significant, though not systematic, model errors. The monthly average S values from January through December were 58, 63, 69, 65, 64, 60, 51, 42, 39, 35, 39 and 51 ppb pvu^{-1}, which are comparable to those reported elsewhere (e.g., Ancellet et al., 1994; Beekmann et al., 1994).

3. Measurement data

To validate the model calculations, we exploit a comprehensive dataset collected within VOTALP,

comprising measurements of O_3, relative humidity (RH) and ^{7}Be at three high-Alpine peak stations (Jungfraujoch (3580 m asl), Sonnblick (3106 m) and Zugspitze (2962 m)) and at Mt. Cimone (2165 m), the highest peak in the Northern Apennines, O_3 and meteorological data from a number of lower sites, total column O_3 measurements, O_3 soundings, and water vapor (WV) satellite images.

WV satellite images are ideal for depicting the spatial extension of tongues of dry air penetrating from the stratosphere into the troposphere. These streamers can be identified in radiance measurements of the Meteosat satellite in the 6-μm WV channel (Appenzeller and Davies, 1992; Appenzeller et al., 1996a; Wirth et al., 1997) and show up as dark regions in the WV images which constitute a weighted average of the water vapor content in the middle and upper troposphere. If the upper troposphere is very dry, the maximum sensitivity of the instrument is centered at approximately 450 hPa; in a relatively moist upper troposphere, it is shifted to somewhat higher levels. Other factors, such as the temperature profile and the viewing angle, also influence the level of maximum sensitivity (Fischer et al., 1982). To compare our model results with the satellite images, we computed a weighted average of the stratospheric-air-tracer mass between 4000 m and 11 000 m asl. The weighting function with a maximum weight between 6000 and 8000 m asl resembles a typical sensitivity profile of the Meteosat instrument.

Dark regions in the WV radiance images are not in all cases due to stratospheric intrusions. Sometimes, they merely show dry portions of upper tropospheric air. Therefore not all features which are seen in the images have a counterpart in the tracer simulations, but calculated high stratospheric tracer concentrations in the troposphere should always appear as dark areas.

The most important measurements, which are later used also for studying the seasonal variation of stratospheric intrusions independently from the model calculations, were carried out at the high mountain sites (see Fig. 1). Stratospheric air has certain characteristics, which can be used for its detection in the troposphere. Since O_3 concentrations are much higher in the stratosphere than in the troposphere, intrusions of stratospheric air are initially rich in O_3, but mixing and dilution with tropospheric air destroys this feature over the time. Humidity drops to low levels during intrusions, but it is debatable which humidity measure is most appropriate for identifying stratospheric intrusions. In principle, specific humidity would be best, since it is conserved in an air mass. However, stratospheric air masses usually mix with tropospheric ones in the process of descending to the lower troposphere. Since specific humidity in tropospheric air is highly variable, with low values in winter and at high altitudes and high values in summer and close to the surface, any fixed threshold for specific humidity would artificially lead to the identification of more intrusions in winter and at the higher stations. For this reason, the observational climatology is based on RH, which is less variable in the troposphere. However, low RH may also be encountered in air that has descended from the upper troposphere undergoing adiabatic warming. RH may thus be used to identify stratospherically influenced air, but it is not a stratospheric air tracer.

^{7}Be is a cosmogenic radionuclide with a radioactive decay half-life of 53 days that is formed in the stratosphere and upper troposphere and attaches to aerosols. Although high concentrations indicate downward transport (Koch and Mann, 1996), ^{7}Be is not a specific stratospheric tracer, because one third is produced in the troposphere and because it is subject to wet scavenging by precipitation. Less than 40% of the tropospheric ^{7}Be (Koch et al., 1996) and only 25% of that at the surface (Dutkiewicz and Husain, 1985) originates from the stratosphere. Some authors (e.g., Baskaran, 1995) propose that surface ^{7}Be concentrations reflect the variation in tropospheric transport and removal processes rather than variations in STE. In addition, we have ^{7}Be data only with a time resolution of 24 and 48 h, whereas stratospheric intrusion episodes are sometimes much shorter. An analysis of ^{7}Be data from Jungfraujoch was recently presented by Zanis et al. (1999).

There are a few more indicators for stratospheric intrusions, for instance low carbon monoxide (CO) or radon 222 concentrations (both of which have their main source at the ground), but none of them was available at all stations involved in this study. Therefore, for the observational climatology presented later we do not use these data. The ^{7}Be samples were taken over 24 h at all sites except Jungfraujoch where only 48-h samples were available. For O_3 and RH, 1-h averages were used. See Table 1 for the time periods with available data.

4. Case studies

4.1. Episode of 4 October 1996

As a first illustration of the model results, Fig. 2 shows the O_3 tracer mixing ratios in the Sonnblick grid cell for a 50-day period starting on 7 September 1996 taken from the three-year model run, along with the measured concentrations of O_3 and ^{7}Be. The model simulates several episodes with strong stratospheric influence. The two most intense episodes with directly descending stratospheric air (days 27 and 48) correspond well with distinct peaks in ^{7}Be and O_3. Also the episode on day 10, caused by horizontal advection of aged stratospheric air, is in good agreement with the measurements. Two extremely short incidents of the stratospheric O_3 tracer (days 42 and 43) go along with spikes in the measured O_3 concentrations.

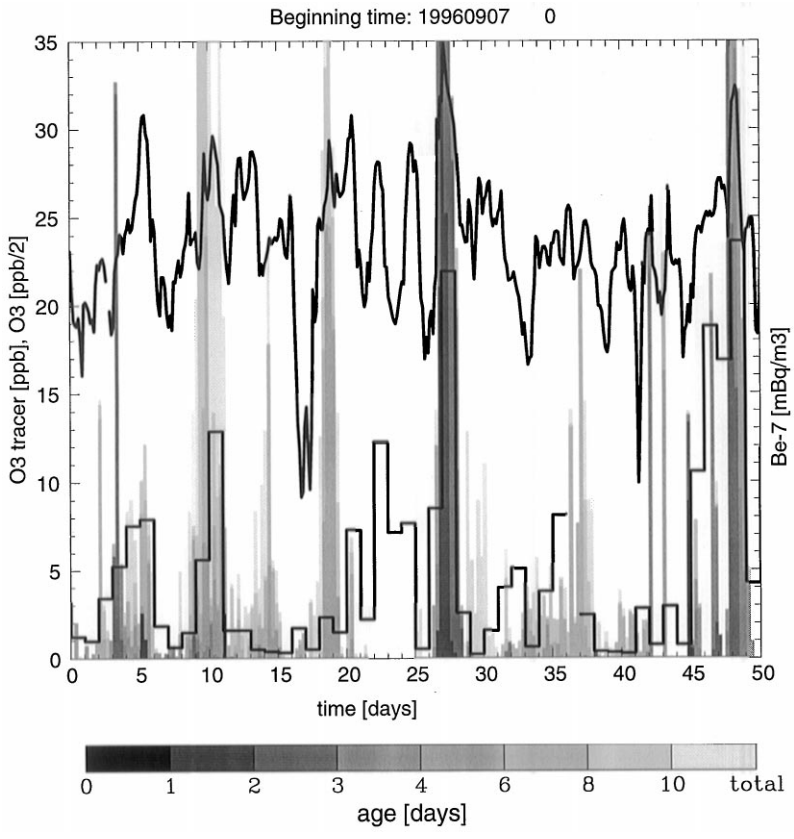

Fig. 2. Mixing ratios of the stratospheric ozone tracer during 7 September 1996 to 27 October 1996 in the Sonnblick grid cell. The color code gives the relative contributions of air of different tropospheric age classes (with age defined as the time since a particle crossed the tropopause). Also shown are the measured ozone mixing ratios (in ppb/2) (upper line) and the ^{7}Be concentrations (lower line) at Sonnblick.

The episode with high modeled tracer mixing ratio on day 19 is accompanied by an O_3 peak, but not by a ^{7}Be peak at the stations. Back trajectory analyses and inspection of weather maps revealed that the air mass experienced precipitation before arriving at Sonnblick. Obviously, ^{7}Be-carrying aerosols were washed out. During an episode of high ^{7}Be concentrations (day 23), the model results suggest no stratospheric influence and also the rather smooth variation in measured O_3 is not typical for a stratospheric intrusion. Back trajectory analyses showed that in this case the air came from the free troposphere over the Atlantic ocean and was not affected by precipitation during the last few days prior to arrival. This probably sufficed to produce the high ^{7}Be concentrations. In the following, we study the strongest episode on day 27, i.e., on 4 October, in more detail.

4.1.1. Observations and synoptic situation

On 3 and 4 October 1996, high daily ^{7}Be concentrations were observed at Sonnblick, Zugspitze and Jungfraujoch (Fig. 3b). O_3 mixing ratios showed sharp spikes of about 72 ppb at all three sites (Fig. 3b), with the maximum at the westernmost station (Jungfraujoch) occurring more than half a day before the maximum at Sonnblick. At the same time, RH dropped to very low values (Fig. 3a). These data suggest that an intrusion of stratospheric air, progressing from the west to the east, passed the three stations.

The weather pattern during this episode was characterized by an upper-level cold trough, located to the north of France on 1 October (Berliner Wetterkarte) and propagating eastwards during the following days. On 2 October, a low was cut off, as shown in a plot of PV on the 310 K isentropic surface (Fig. 4a). The cut-off low was prominent also in the surface weather charts and became almost stationary over the Gulf of Genoa – a preferred region for cyclogenesis – on 3 to 5 October (Fig. 4b). Rain showers associated with thunderstorms were observed in southern Italy and Tunisia, which were facilitated by the reduction of static stability beneath the descending PV-rich stratospheric air (Thorpe, 1997). Heavy rainfall was also observed in parts of the Alps.

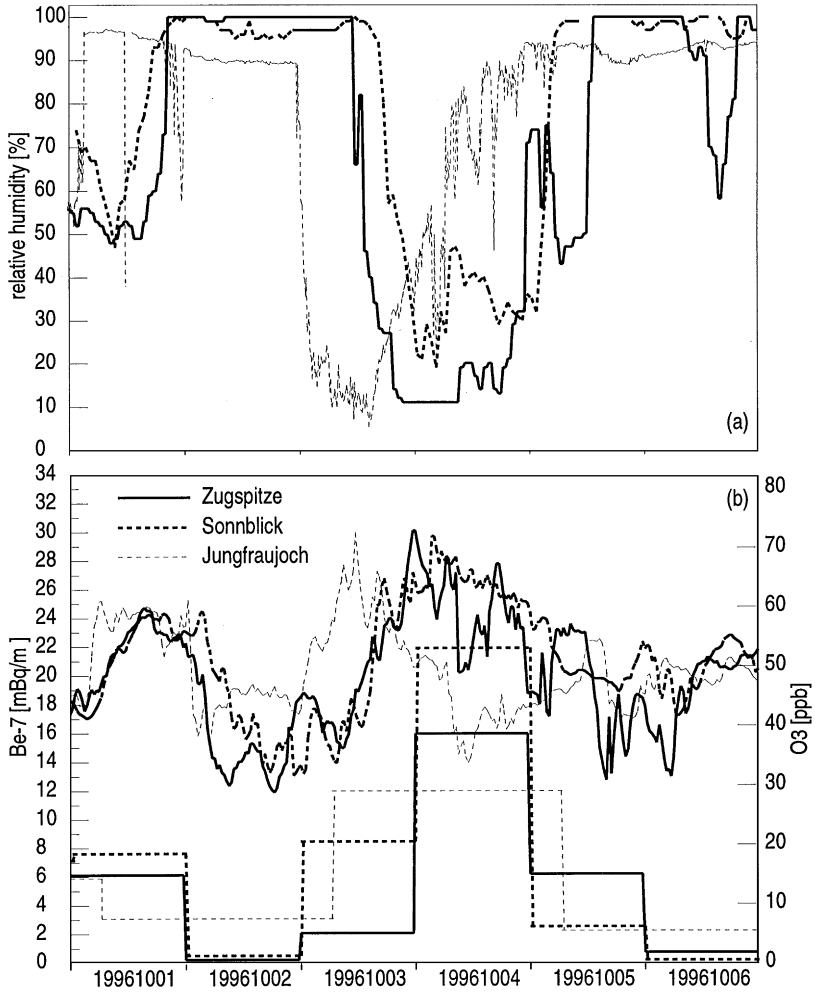

Fig. 3. RH (a), and O_3 and ^{7}Be concentrations (b) at Jungfraujoch, Zugspitze and Sonnblick during 1–5 October 1996. The daily average levels in (b) refer to ^{7}Be.

To depict the spatio-temporal behavior of the intrusion of stratospheric air into the troposphere, we employed the coherent-ensemble-of-trajectories (CET) method of Wernli and Davies (1997). We calculated three-dimensional forward trajectories initialized on 30 September at 18 UTC in the whole model domain every $1^\circ \times 2^\circ$ at heights of 7000, 8000, 9000 and 10000 m asl. From all trajectories we selected a subset that started with PV > 1.6 pvu and descended by more than 5000 m during the following 120 h, i.e., those representing an intrusion of stratospheric air into the lower troposphere. A broad zone of descending air originating between southern Greenland and eastern Scandinavia was found (Fig. 5).

To test how well FLEXPART simulates the transport processes during this episode, we reinitialized it on 28 September at 0 UTC to avoid confusion with older tracer structures. In the following, we discuss the model results not strictly in chronological order, but in three stages, using different methods to check the validity of our simulations: For the upper troposphere, we compare the tracer patterns with WV images and with total column O_3 measurements. For the middle to lower troposphere, we check our results with measurement data from the mountain peak observatories. Finally, we study O_3 and RH measurements at various sites.

4.1.2. Upper troposphere

On 1 October 12 UTC, several dry regions were identifiable in the WV image (Fig. 6a). Of these, the one stretching from north of Ireland to the west of Spain reached the Alps two days later. The dry region is matched well by an intrusion of stratospheric air found in the model results (Fig. 6b). Even several secondary minima in the WV content within the intrusion correspond to local

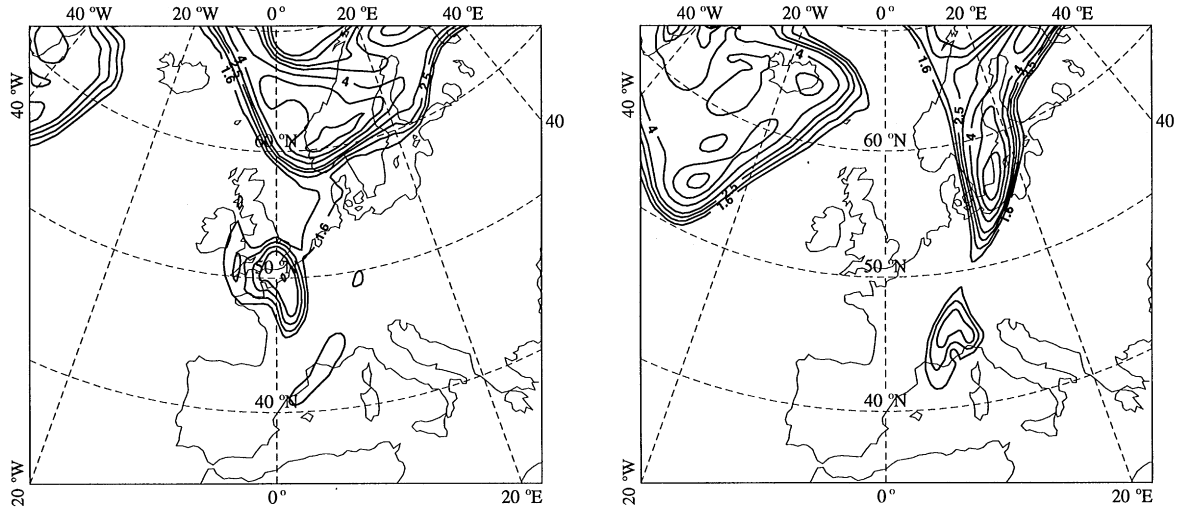

Fig. 4. Isentropic PV on the 310 K surface on 2 October 1996 0 UTC (a) and 3 October 0 UTC (b) taken from ECMWF analyses. The contour lines shown are 1.6, 2, 2.5, 3, 4, 5 and 6 pvu.

maxima of the stratospheric tracer (one north-west of Ireland, another over southeastern England, and one over France), but the driest region to the west of Spain is almost missing in the model results. Probably this air originated at heights just below the tropopause.

Two days later, on 3 October 12 UTC, the dry intrusion had just passed the Alps (Fig. 6c). The elongated structure stretched from southern Scandinavia to Algeria, which is reflected in the model results (Fig. 6d). The driest regions over Algeria and over Poland are particularly well predicted. The modeled intrusion is somewhat broader than the observed one, but this is due to the 3-h averaging. On 3 October, the intrusion of stratospheric air also appeared as a finger of high total O_3 column in plots of TOVS satellite measurements (not shown) prepared by the National Center for Environmental Prediction (NCEP), as in the study of Davies and Schuepbach (1994).

24 h later, the dry intrusion showed a very complicated bended structure, which stretched from Siberia to the Black Sea and to the Alps and rolled up in the cut-off low south of Italy (Fig. 6e). The signature in the WV satellite image was very strong, indicating that the dry air had descended deep into the troposphere. In spite of the complicated structure of the dry intrusion, the model results agree very well with the satellite image (Fig. 6f), indicating that the upper tropospheric development was accurately captured by the model.

4.1.3. Alpine peak level

To illustrate the tracer transport in the lower to middle troposphere, we present plots of the average O_3 tracer mixing ratio between 2000 and 4000 m asl (Fig. 7), an altitude range where measurements from the mountain peaks were available (Fig. 3). Two structures, connected with the dry intrusion at higher levels, appeared in the lower troposphere on 2 October 0 UTC (Fig. 7a). They merged and formed a broad zone of high stratospheric O_3 content over whole western Europe one day later (Fig. 7b). This zone moved eastward and was centered over the Alps on 4 October 0 UTC (Fig. 7c), with the highest mixing ratios (up to 100 ppb) located over the eastern Alps. On 5 October 0 UTC, the intrusion (Fig. 7d) was still present over the eastern Alps, but shortly later it moved on. On 5 October 0 UTC, O_3 tracer also appeared at the surface, with the region of maximum impact being located over northern Africa (Fig. 7e).

Fig. 2 shows the time series of the stratospheric O_3 tracer mixing ratio in the Sonnblick grid cell taken from the three-year model run. There was a pronounced peak of 60 ppb in the morning hours on 4 October, exactly when the measured O_3 mixing ratios reached their maximum value (72 ppb). The air consisted of stratospheric air, 1–3 days old, with a maximum mixing ratio of 50% (not shown). An admixture of 50% background tropospheric air containing around 30 ppb of O_3 would explain the discrepancy between the O_3 tracer and the observed O_3 mixing ratio.

Modeled O_3 tracer mixing ratios at Zugspitze behaved similarly as those at Sonnblick, but the maximum value was lower (45 ppb). Maximum measured O_3 mixing ratios were the same as at Sonnblick, but the duration of the O_3 peak was shorter, consistent with the lower ^{7}Be

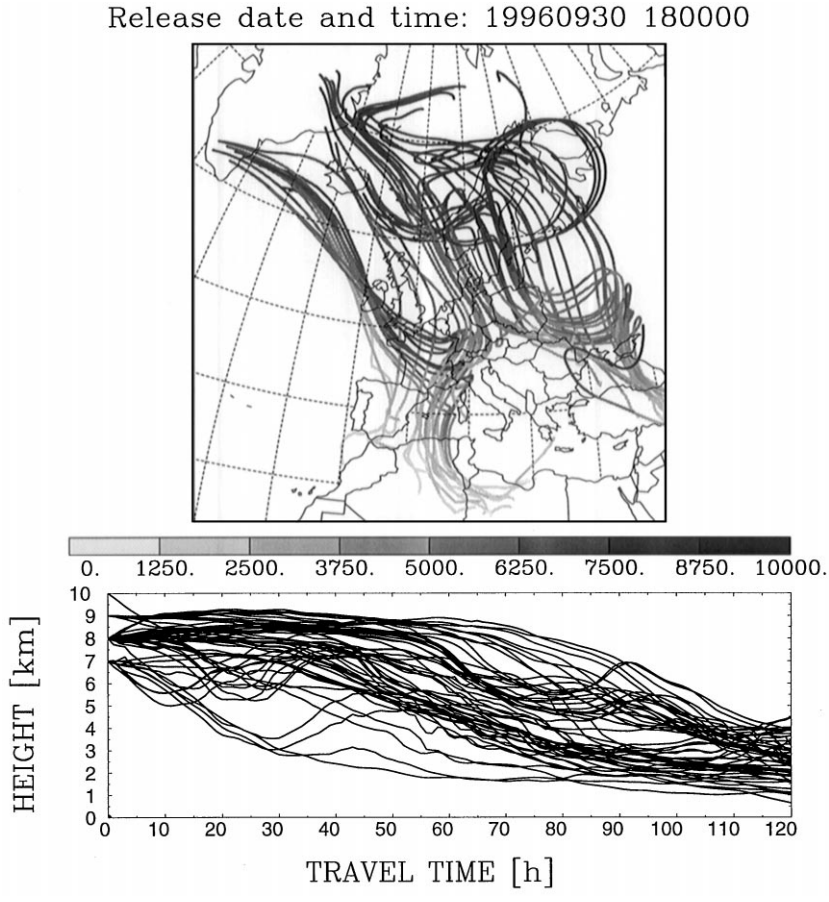

Fig. 5. Illustration of the coherent ensemble of trajectories that demarcates the pathway of the stratospheric air into the troposphere during the first days of October 1996. The trajectories were initialized on 30 September 18 UTC. Only those that started in the stratosphere and descended by more than 5000 m are shown. The upper plot shows the horizontal projection of the trajectories with the shading indicating the height (in m). The lower plot shows the corresponding time-height profile of the trajectories.

concentrations. At Jungfraujoch, tracer mixing ratios started to increase one day earlier and peaked at 35 ppb on 3 October 12 UTC. This timing is in good agreement with the measurements.

Fig. 8 shows a time-height plot of the O_3 tracer mixing ratio at the location of Hohenpeißenberg (Fig. 8), which is at the northern edge of the area where the intrusion reached the surface (compare Fig. 7e). An O_3 sonde, launched at Hohenpeißenberg on 4 October at 5 UTC revealed a dry ozone-rich (67 ppb) layer between 1500 and 3000 m asl sandwiched between much moister air masses with lower O_3 concentrations. This compares very well with the model results that showed O_3 tracer mixing ratios of 5 to 50 ppb between 1500 and 2500 m.

4.1.4. Low altitudes

Measurements of humidity and O_3 from other stations within the Alps show that the stratospheric intrusion was

Fig. 6. Comparison between the WV images and the results of the stratospheric tracer calculations. Dark areas in the WV images represent dry areas, colors show the land–sea distribution. The tracer columns are a weighted average of the tracer mass between 4000 m and 11000 m asl and are given in arbitrary units. Shown are the WV images on 1 October 12 UTC (a), the 3-h average tracer columns on 1 October 12–15 UTC (b), the WV image on 3 October 12 UTC (c), the 3-h average tracer columns on 3 October 12–15 UTC (d), the WV image on 4 October 12 UTC (e) and the 3-h average tracer columns on 4 October 12-15 UTC (f). Note that the map projections are not identical.

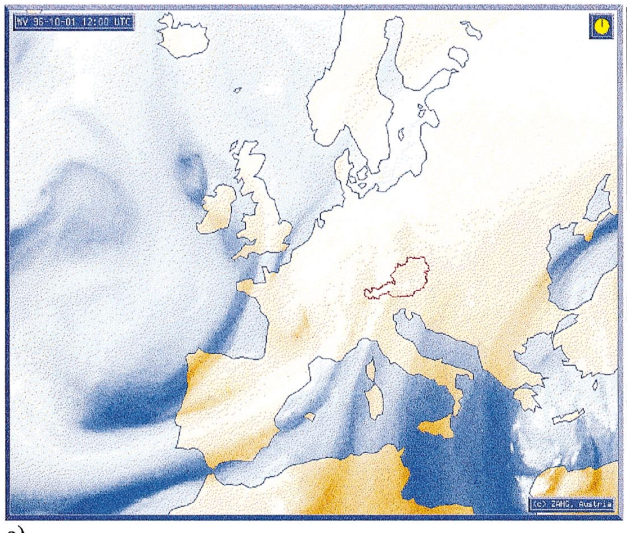
NV 96-10-01 12:00 UTC
(c) ZAMG, Austria

a)

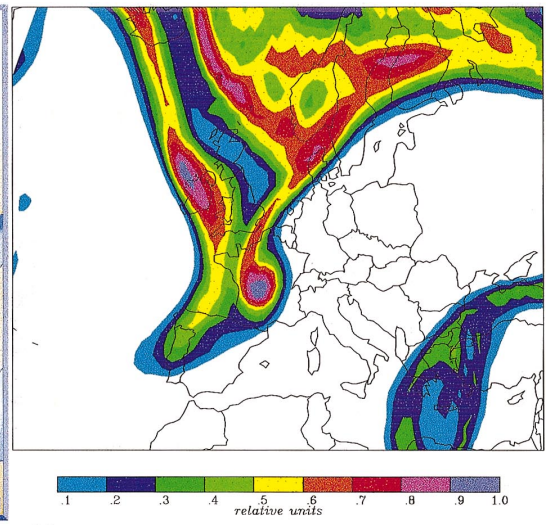
.1 .2 .3 .4 .5 .6 .7 .8 .9 1.0
relative units

b)

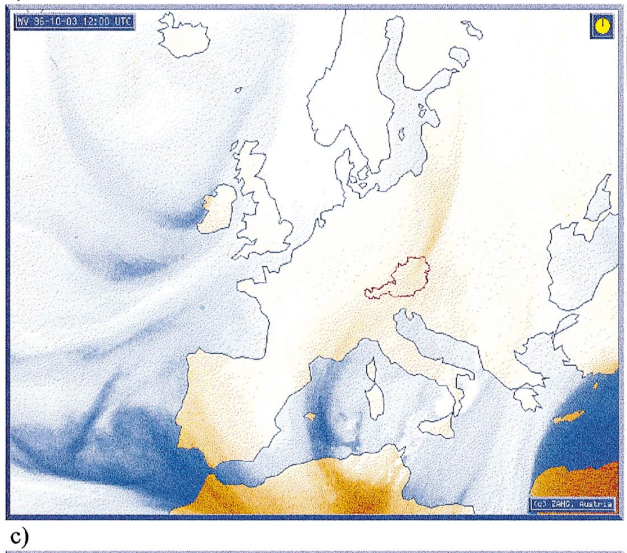
NV 96-10-03 12:00 UTC
(c) ZAMG, Austria

c)

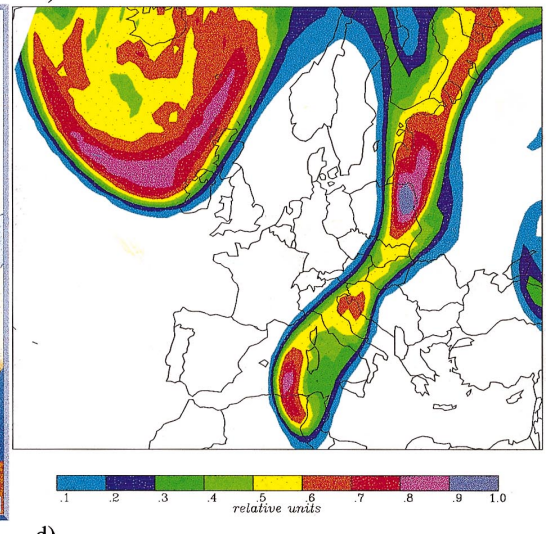
.1 .2 .3 .4 .5 .6 .7 .8 .9 1.0
relative units

d)

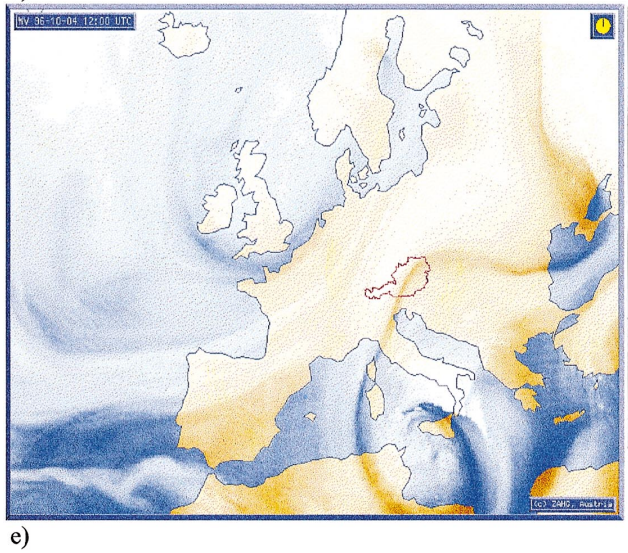
NV 96-10-04 12:00 UTC
(c) ZAMG, Austria

e)

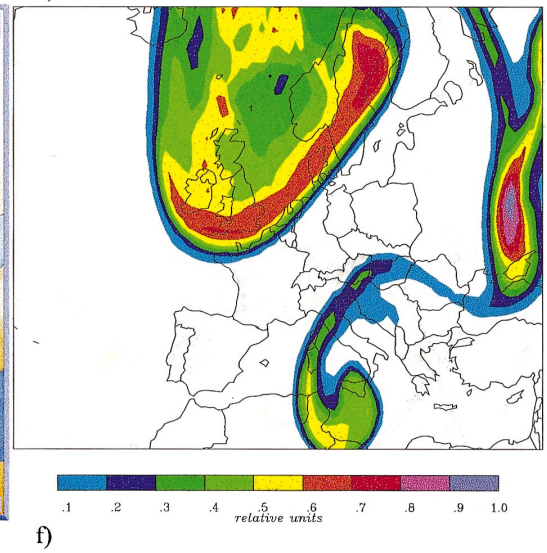
.1 .2 .3 .4 .5 .6 .7 .8 .9 1.0
relative units

f)

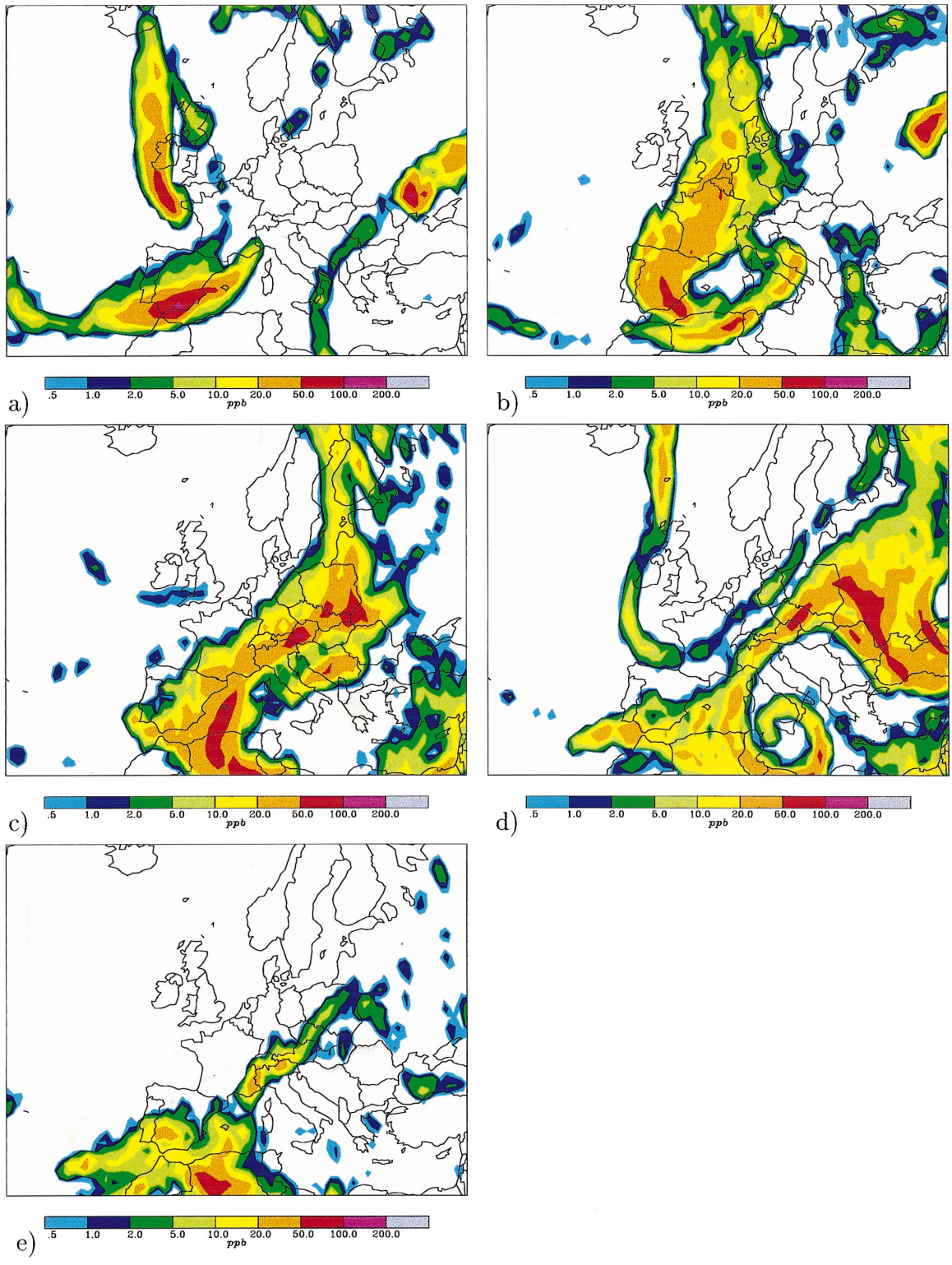

Fig. 7. Average O_3 tracer mixing ratio between 2000 and 4000 m on 2 October 0–3 UTC (a), 3 October 0-3 UTC (b), 4 October 0–3 UTC (c), 5 October 0–3 UTC (d), and the average tracer mixing ratio between the surface and 2000 m on 5 October 0–3 UTC (e).

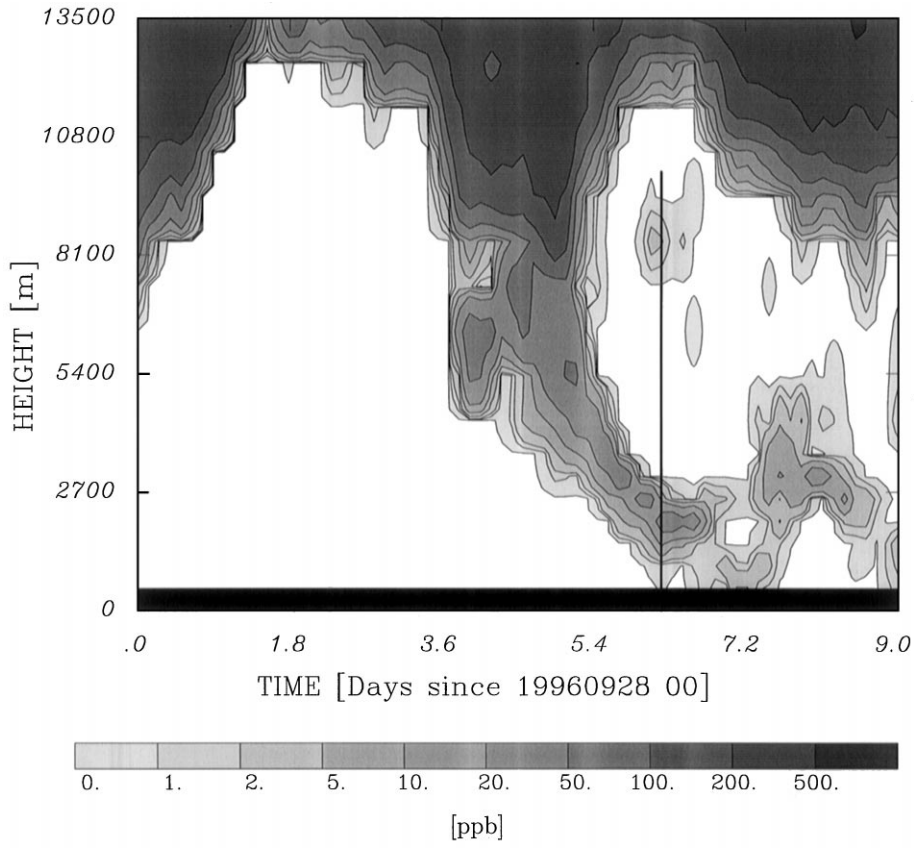

Fig. 8. Time–height diagram of the modeled ozone tracer mixing ratios at Hohenpeißenberg. The black area indicates the height of the model topography, the vertical black line marks the time of the ozone sounding at Hohenpeißenberg.

indeed detectable below 3000 m. At the Wank mountain site (1776 m), neighboring the Zugspitze, there was clear evidence that the intrusion reached that level. RH dropped to 25%, while O_3 rose by 15 to 60 ppb some hours after the peak at the Zugspitze. At Davos (1640 m) RH dropped to 15%, while O_3 rose by 15 ppb to 50 ppb. At lower sites the signal of the intrusion got less clear, since it was overlaid by pronounced diurnal variations. However, practically all of the Alpine sites considered showed low humidity and moderately high O_3 concentrations. At Gaisberg Zistelalm (1010 m) and St. Koloman (1006 m), for instance, drops in RH were associated with O_3 peaks.

4.2. *Episode from 27 May to 6 June 1996*

4.2.1. *Synoptic situation*

On 27 May 1996, a trough in the 500 hPa chart was located to the north-west of Scandinavia (Berliner Wetterkarte), where stratospheric PV values were found on the 310 K isentropic surface (Fig. 9a). On 28 May, the trough extended southwards to Italy, and a tongue of high PV was generated (Fig. 9b). One day later, a low was cut off over the eastern Mediterranean, which intensified during 30 May and then slowly propagated eastwards. Applying again the method of Wernli and Davies (1997) by selecting all trajectories that started in the stratosphere on 27 May at 0 UTC and descended by more than 5000 m, we obtained a CET that demarcates a narrow pathway of stratospheric air crossing the eastern Alps (Fig. 10).

At the surface, an anticyclone developed over Central Europe on 29 May, persisting until 1 June, when a disturbance passed. But even during the passage of this disturbance, surface winds in southern Europe were weak, and the high pressure area was re-established soon after. This is important because stratospheric air, previously conveyed to the lower troposphere, persisted in the area for more than a week and was mixed with stratospheric air brought down in a cut-off low several days later.

A second intrusion event started on 2 June (Fig. 9c). On 3 June, a prominent trough in the 500 hPa chart stretched from Scotland to Algeria. At its southernmost

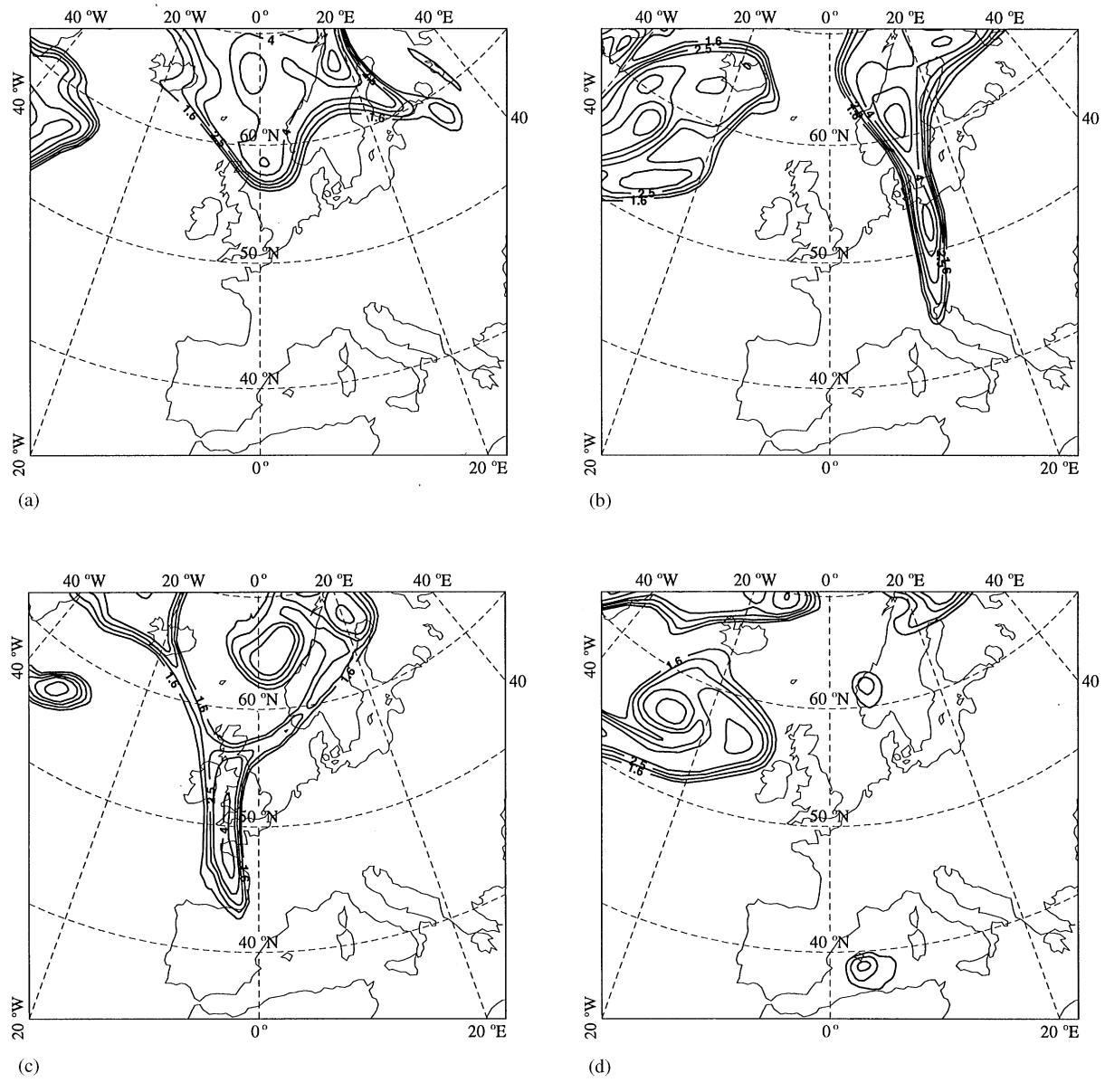

Fig. 9. Isentropic PV on the 310 K surface on 27 May 1996 12 UTC (a), 28 May 1996 12 UTC (b), 2 June 1996 12 UTC (c) and 3 June 1996 12 UTC (d) taken from ECMWF analyses. The contour lines show 1.6, 2, 2.5, 3, 4, 5 and 6 pvu.

tip, a vortex, clearly visible in the infrared satellite image and in the PV chart (Fig. 9d), developed over the Gulf of Genoa. It was cut off on 4 June and slowly advanced southeastwards on 5 and 6 June.

4.2.2. Upper troposphere

Again, we check the FLEXPART (initialized on 25 May at 0 UTC) results in the upper troposphere with WV images. On 29 May 0 UTC, a slender streamer of dry air stretched from southern Scandinavia to southern Italy (Fig. 11a), where it rolled up in the cut-off low that just began to develop. The counterpart of this streamer in the tracer plots was a narrow band of stratospheric air (Fig. 11b), with the 0.4 units contour corresponding well with the position of the streamer. Secondary tracer maxima, like the one over the Baltic Sea, appeared as darker regions in the WV images.

36 h later, the streamer had broken up, indicating that the air had been drawn down irreversibly from the stratosphere. The cut-off low located in the eastern Mediterra-

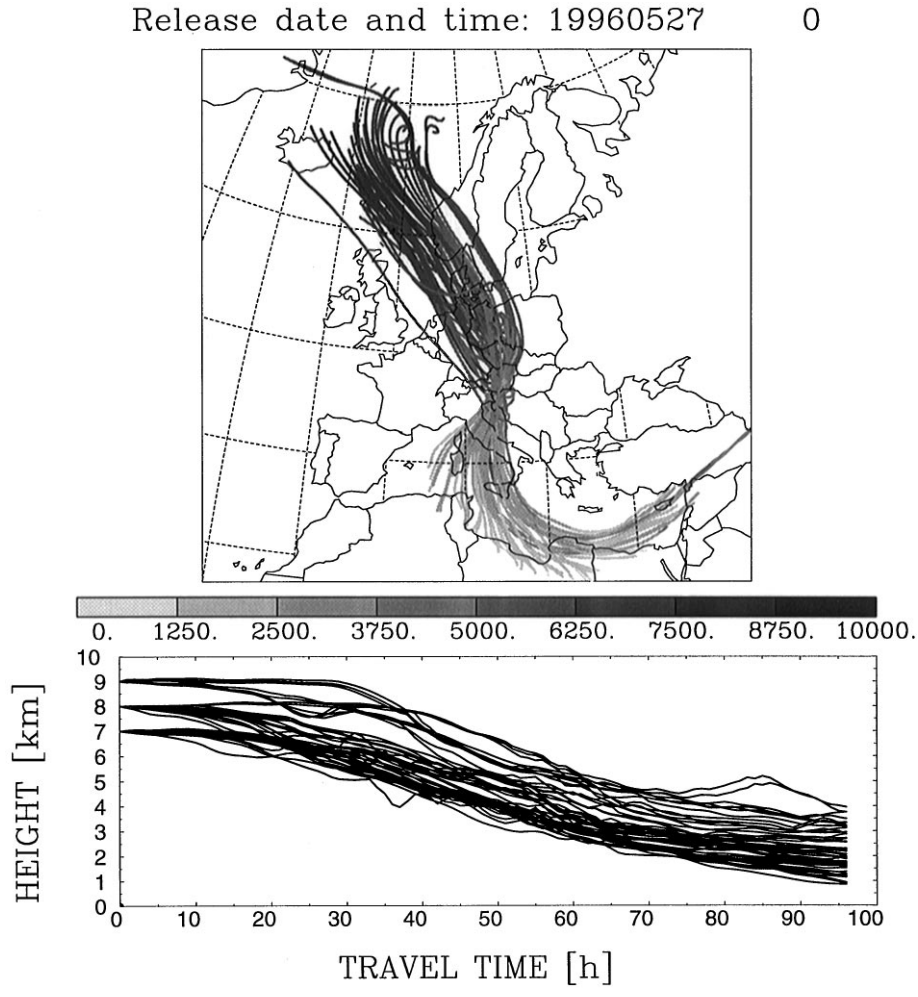

Fig. 10. Illustration of the coherent ensemble of trajectories that demarcates the pathway of the air in the tropopause folding on 29 May. The trajectories were initialized on 27 May 0 UTC and only those are plotted that started in the stratosphere and descended by more than 5000 m. The upper plot shows the horizontal projection of the trajectories with the shading indicating the height (in m). The lower plot shows the corresponding time-height profile of the trajectories.

nean Sea was noticeable as a vortex of dry air in the WV images (Fig. 11c) and its position agreed well with the tracer plot (Fig. 11d). Four days later, on 3 June 18 UTC, the decaying cut-off low was still visible at the southeastern edge of the WV image (Fig. 11e). A second streamer of dry air had formed that stretched from Scandinavia to the east coast of Spain, where it rolled up. The position of the streamer and of the cut-off low were again well matched by the structures in the tracer plots (Fig. 11f) although the delicate structures of the cut-off low were not resolved by the model. During the following two days, the cut-off low moved eastward, and air of stratospheric origin moved down to lower levels in the surface high centered over Central Europe.

An inspection of TOVS total column O_3 measurements provided further evidence for the intrusion: On 28 May, a tongue of up to 380 Dobson units (DU) stretched southwards to Italy, compared to the 300–330 DU observed before. On 29 May, this tongue detached from the main body of high O_3 content. Total O_3 measurements at Sonnblick (Weihs et al., 1999) showed an increase from 319 DU to 385 DU between 26 May to 28 May and a sharp decline to 314 DU on 29 May. At that time, most of the intruded O_3 had obviously passed Sonnblick and the tropopause height over Sonnblick had increased, consistent with the behavior of the modeled tracer concentrations in the upper troposphere (Fig. 11b). The second stratospheric intrusion on 3 June was also accompanied by a tongue of high column O_3.

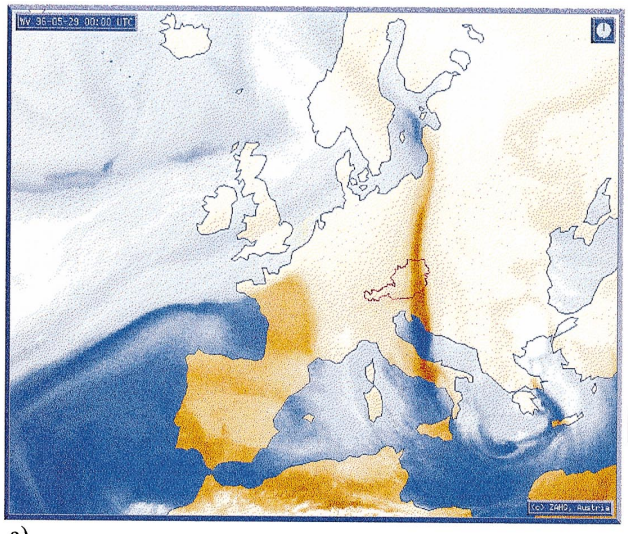
MV 96-05-29 00:00 UTC
(c) ZAMG, Austria

a)

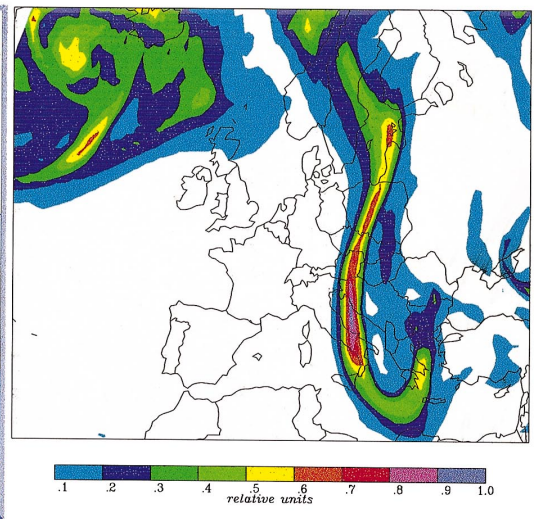
.1 .2 .3 .4 .5 .6 .7 .8 .9 1.0
relative units

b)

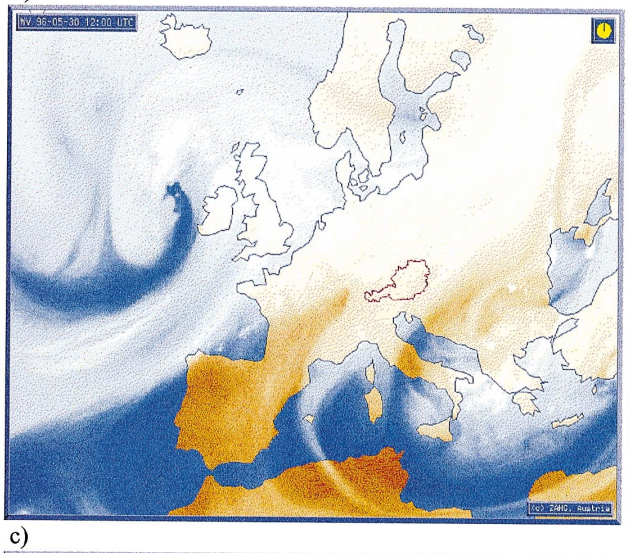
MV 96-05-30 12:00 UTC
(c) ZAMG, Austria

c)

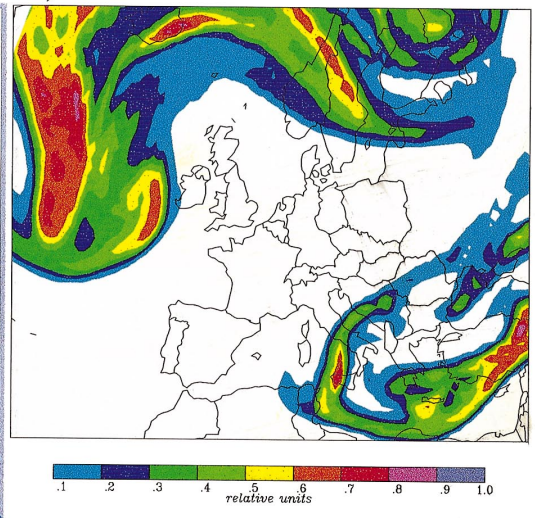
.1 .2 .3 .4 .5 .6 .7 .8 .9 1.0
relative units

d)

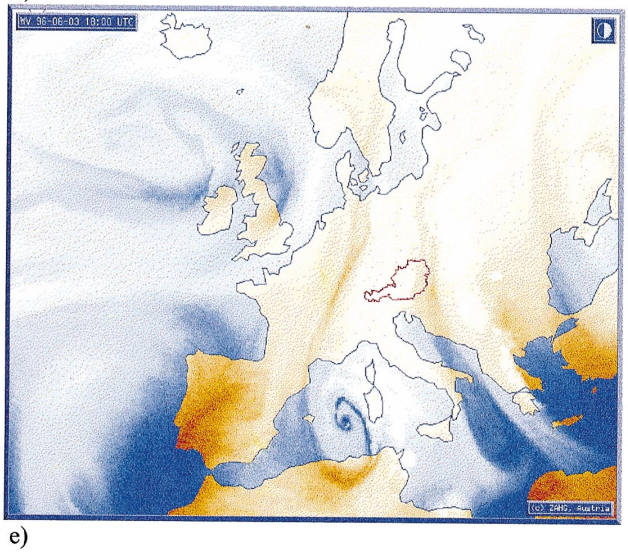
MV 96-06-03 18:00 UTC
(c) ZAMG, Austria

e)

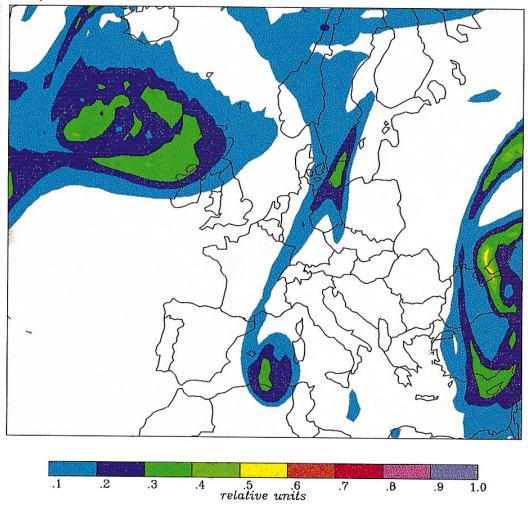
.1 .2 .3 .4 .5 .6 .7 .8 .9 1.0
relative units

f)

4.2.3. Alpine peak level

Again, we consider the average tracer mixing ratios between 2000 and 4000 m asl (Fig. 12). A first blob of stratospheric air with up to 20 ppb O_3 tracer arrived on 27 May at 12 UTC in the Alpine region (Fig. 12a). A trace-back of this isolated blob revealed that it extruded from the stratosphere on 25 May south of Greenland; then it was advected almost horizontally in the troposphere. According to the model results, only the westernmost parts of the Alps were affected by this blob; and no increase in O_3 or ^{7}Be was recorded at the measurement sites.

One day later, on 28 May at 12 UTC, the main intrusion discussed here appeared as a filament of high O_3 tracer mixing ratio stretching from west of Scandinavia to the Alps (Fig. 12b). Note the similar shape compared to the CET seen in Fig. 10, although the CET reflects a time–space relation, whereas Fig. 12b is an instantaneous snapshot. At that time, the blob of aged stratospheric air was still isolated from the "fresh" stratospheric air, but the two structures merged 12 h later. There was a clear spike in the O_3 mixing ratio at Jungfraujoch in the evening of the 28th, coinciding with high ^{7}Be concentrations (Fig. 13) and low concentrations of radon 222 (not shown). These data, in contrast to the model results, evidence that the stratospheric air reached Jungfraujoch. The stratospheric O_3 tracer fields show that the modeled intrusion was erroneously located 200 to 300 km to the east, which must be due to a spatial shift in the ECMWF analyses.

At 12 UTC on 29 May (Fig. 12c), O_3 tracer mixing ratios reached their highest values (up to more than 100 ppb). According to the model results, the Zugspitze peak was just missed by the intrusion, while the measurements at this site showed elevated O_3 and ^{7}Be concentrations and a dip in the humidity, in agreement with O_3 lidar measurements in nearby Garmisch-Partenkirchen (Eisele et al., 1999). O_3 sounding at Hohenpeißenberg, 50 km north of Zugspitze, on 29 May at 6 UTC (not shown) revealed a dry layer (RH less than 10%) between 1700 and 3100 m with maximum O_3 mixing ratios of 75 ppb. In the model results, a corresponding layer at the same height was found approximately 200 km further to the east, again suggesting a horizontal displacement of the modeled intrusion.

Consistent with the eastward propagation of the stratospheric air as indicated by the model results, a jump in the O_3 mixing ratio at Sonnblick occurred several hours after that at Zugspitze (Fig. 13). The maximum O_3 mixing ratios at the three Alpine peaks were at about the same level, suggesting that they all received air of similar origin. After the passage of the intrusion, all three sites showed a sudden decrease of O_3 and an increase in humidity. Trajectory calculations revealed that they received air from the mid-Atlantic boundary layer during a few hours.

Finally the subsiding stratospheric air got almost stationary south of the Alps. In the northern Apennines, simulated O_3 tracer mixing ratios were elevated for the next days (Fig. 12d–f). Fig. 14 shows the simulated stratospheric O_3 tracer mixing ratios in the Mt. Cimone grid cell. After two maxima in the tracer mixing ratio caused by the blob of aged stratospheric air on 27 and 28 May, air from the main intrusion arrived late on 29 May. Initially, a significant fraction of this stratospheric air was less than one day old. Modeled O_3 tracer mixing ratios are too low at Mt. Cimone to explain the high measured O_3 concentrations. Note, however, that in the model results the intrusion was horizontally displaced as mentioned before. O_3 tracer mixing ratios 200 km to the east of Mt. Cimone were two times higher than at the location of Mt. Cimone.

Nevertheless, the model results are in relatively good agreement with the measurements. Very high ^{7}Be concentrations measured both on 30 and 31 May confirm the stratospheric nature of this event. Both CO concentrations and RH were low on 30 May, the time of the first tracer maximum. RH dropped to almost zero during the morning hours of 31 May. On 31 May, O_3 mixing ratios of up to 90 ppb were measured, but several peaks in the CO concentrations indicate that polluted boundary-layer air was also present, which possibly led to significant photochemical O_3 production. This is in agreement with observations at Zugspitze that likewise showed a positive relationship between variations of O_3 and CO. A detailed interpretation of the measurements obtained at Mt. Cimone during this episode is presented by Bonasoni et al. (1999).

On 31 May, 12 UTC (Fig. 12d), the signatures of three stratospheric intrusions were present over Europe. The structures over southern Europe, the Mediterranean Sea and northern Africa belonged to the intrusion and cut-off low previously discussed and formed a reservoir layer south of the Alps at a height of 2000 to 3000 m asl. This air mass was swept back towards the Alps during the following days, yielding a very complicated tracer pattern

Fig. 11. Comparison between the WV images and the results of the stratospheric tracer calculations. The tracer columns are a weighted average of the tracer mass between 4000 m and 11000 m asl and are given in arbitrary units. Shown are the the WV images on 29 May 0 UTC (a), the 3-h average tracer columns on 29 May 0–3 UTC (b), the WV image on 30 May 12 UTC (c), the 3-h average tracer columns on 30 May 12–15 UTC (d), the WV image on 3 June 18 UTC (e) and the 3-h average tracer columns on 3 June 18–21 UTC (f). Note that the map projections are not identical.

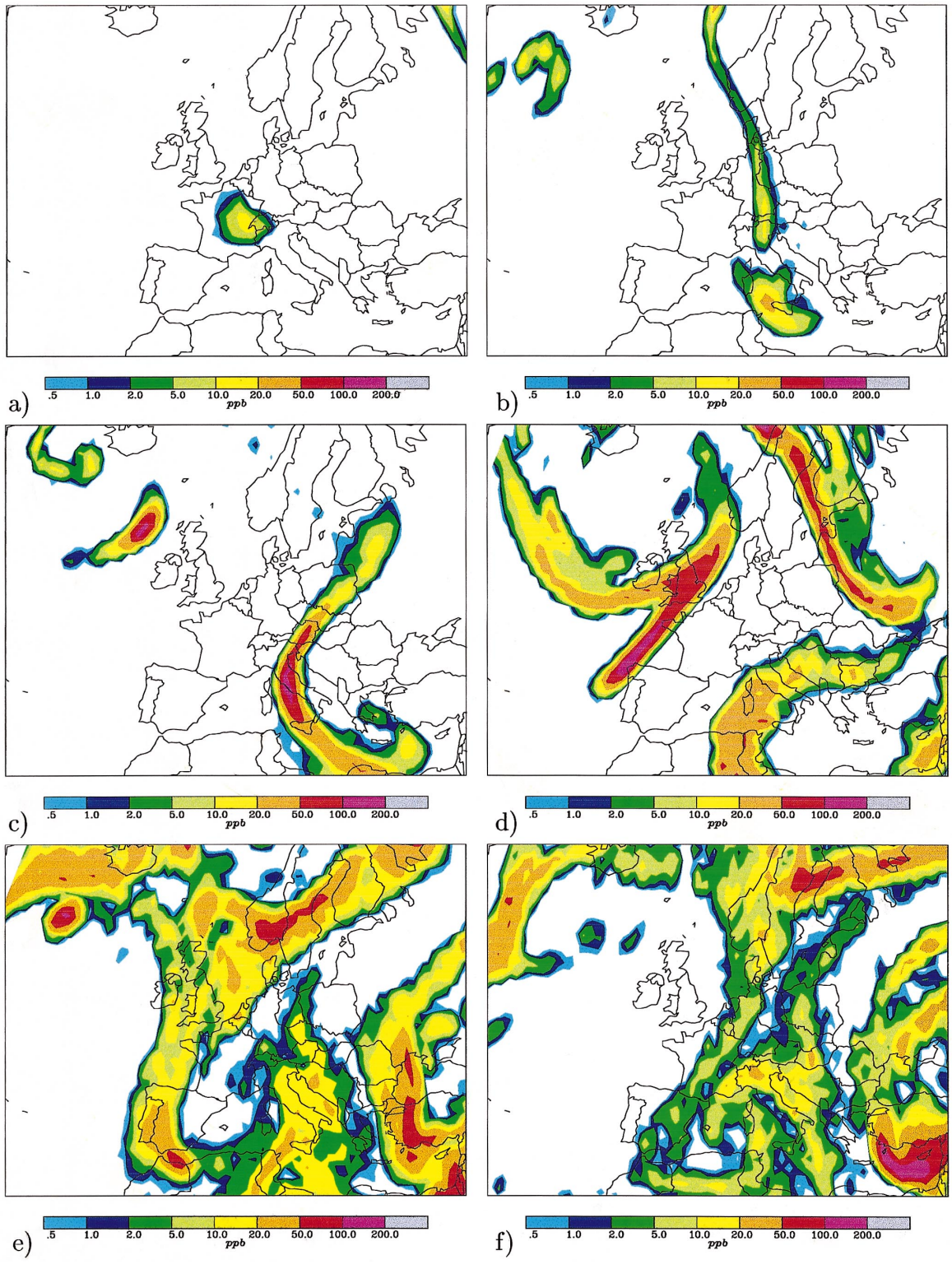

Fig. 12. Average O_3 tracer mixing ratios between 2000 m and 4000 m on 27 May 12–15 UTC (a), 28 May 12–15 UTC (b), 29 May 12–15 UTC (c), 31 May 12–15 UTC (d), 3 June 0–3 UTC (e) and 4 June 0–3 UTC (f).

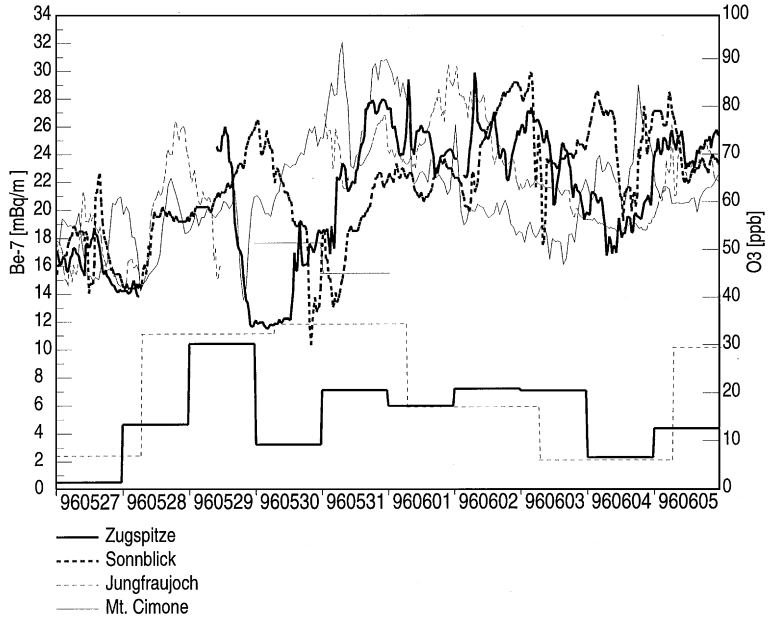

Fig. 13. O_3 and ^7Be concentrations at Jungfraujoch, Zugspitze and Sonnblick during 27 May to 5 June 1996. The daily average levels refer to ^7Be.

on 3 June, 0 UTC (Fig. 12e). Stratospheric air brought down in the previously discussed cut-off low over western Europe started to mix with the aged stratospheric air already present south of the Alps (Fig. 12f). On 5 June air brought down from the stratosphere in three subsequent intrusion events, occurring within a period of ten days in different regions, was present at Mt. Cimone at the same time (Fig. 14). Meteorological conditions were also conducive to photochemical O_3 formation.

4.2.4. Low altitudes

Radio soundings at several places in the Alpine area showed a layer of dry air at low levels on 29 May; in Munich, for instance, at 880 hPa. Several monitoring sites in the Alps showed an increase in O_3 together with a drop in RH. At the Wank mountain (1776 m), the maximum O_3 concentrations during 29 May were close to those at Zugspitze, and there was a moderate drop in humidity. This was observed shortly after the corresponding event at Zugspitze and is an indication for the subsidence of this air mass. High-resolution O_3 lidar and in situ measurements in nearby Garmisch-Partenkirchen showed a descending ozone-rich (60–80 ppb) layer that reached the lowest lidar level at 200 m above the valley floor and also the ground station (see Eisele et al., 1999).

In Davos (1640 m) O_3 mixing ratios rose from 35 ppb at 2 UTC to 51 ppb at 7 UTC, while RH dropped from 80 to 20%. During daytime, O_3 mixing ratios stayed fairly constant at 52 ppb, and RH decreased to 13%. At Ritten (1770 m) there was a drop in RH to 9% in the morning hours on 29 May, associated with an increase in O_3 to 62 ppb.

Consistent with the eastward motion of the stratospheric air, stations farther to the east showed the drop in RH some hours later. At Gaisberg Zistelalm (1010 m), O_3 increased from 37 to 66 ppb, while RH decreased from 77 to 35%. At Haunsberg (740 m), O_3 increased from 40 to 70 ppb during 29 May, while RH dropped from 65% to 18%. At the slope (1547 m) of the Rax mountain, one of the easternmost peaks of the Alps, O_3 reached a maximum of 62 ppb on 30 May at 6 UTC, 1.5 days after the first peak was observed at Jungfraujoch.

5. Seasonal variation of stratospheric intrusions based on measurement data

5.1. Screening algorithm

Continuous measurements of O_3, RH and ^7Be were carried out at Jungfraujoch, Sonnblick, Zugspitze and Mt. Cimone for several years (Table 1). These data are used to identify days of significant influence of stratospheric intrusions. Since only few ^7Be data were available for Mt. Cimone, the results for this site are not presented. For Sonnblick and Jungfraujoch the database is also rather small so that results for these stations should be interpreted with caution.

In our screening algorithm a day is considered to be an "intrusion day" if (i) the ^7Be concentration is higher

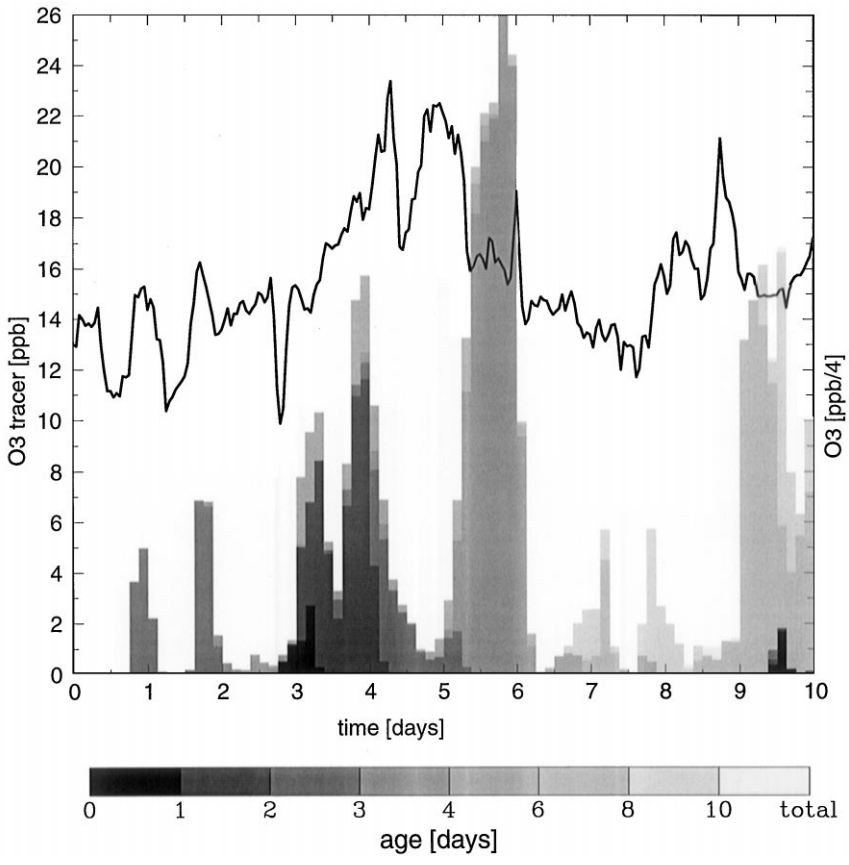

Fig. 14. Mixing ratios of the stratospheric ozone tracer during 27 May 1996 to 5 June 1996 in the Mt. Cimone grid cell. The shading indicates the relative contributions of air of different tropospheric age classes. Also shown are the measured ozone mixing ratios at Mt. Cimone (in ppb/4). The time-axis starts on 27 May at 0 UTC.

Table 1
Periods of measurements used in this study and data availability (%) during these periods. The last line gives the periods and the simultaneous availability (%) of ^{7}Be, O_3 and RH data as required for the observational climatology

	Mt. Cimone		Zugspitze		Sonnblick		Jungfraujoch	
	Period	Availability	Period	Availability	Period	Availability	Period	Availability
^{7}Be	3/96–1/98	5	1/91–9/97	88	6/96–7/98	84	4/96–7/98	92
O_3	3/96–10/97	98	1/91–9/97	93	1/95–7/98	89	1/95–3/98	98
RH	3/96–10/97	97	1/91–12/97	100	1/95–8/98	59	1/95–4/98	99
All data	—	—	1/91–9/97	84	6/96–7/98	85	4/96–3/98	89

than 8 mBq m^{-3}, (ii) the daily minimum RH is lower than 30%, and (iii) the daily maximum O_3 concentration is at least 10% above the monthly mean concentration $\overline{O_3}$. This procedure was set up through subjective analyses of many intrusion episodes. Therefore, the exact threshold values are somewhat arbitrary. Similar thresholds for ^{7}Be and RH were used by Scheel et al. (1999). The additional O_3 criterion was introduced to eliminate cases where the air descended only from the upper troposphere.

The great sensitivity of the results to the choice of the thresholds is shown in Fig. 15, where the annual cycle of

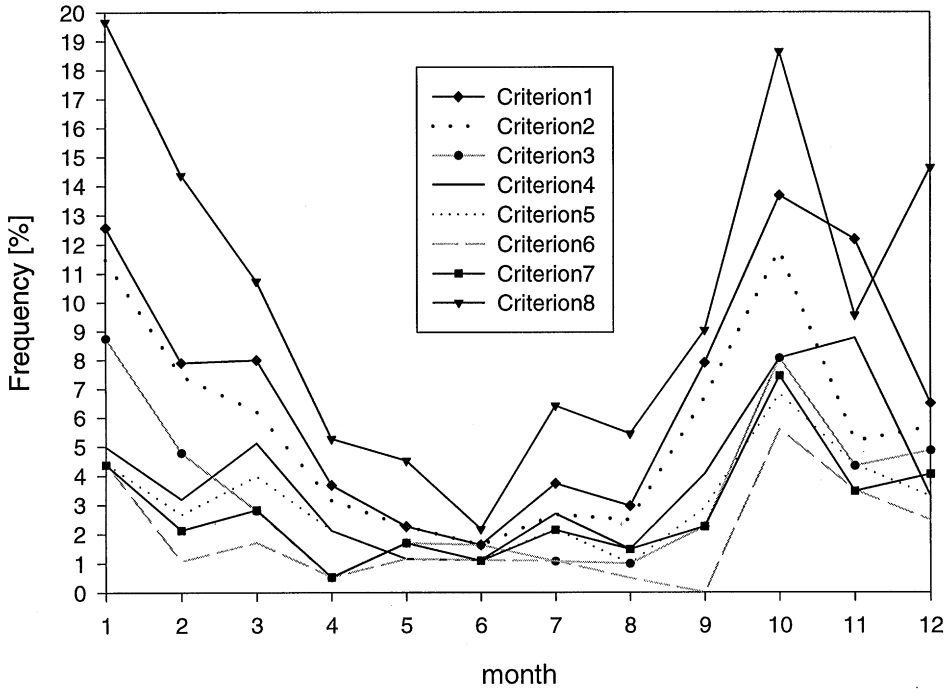

Fig. 15. Seasonal variation of the frequency of stratospheric intrusion days at Zugspitze as obtained with different criteria for ^{7}Be [mBq m^{3}], RH [%] and O_3, which had to be fulfilled simultaneously: 1: $^{7}Be > 8$, $RH < 40$, $O_3 > 1.1 \times \overline{O_3}$, 2: $^{7}Be > 8$, $RH < 30$, $O_3 > 1.1 \times \overline{O_3}$, 3: $^{7}Be > 8$, $RH < 20$, $O_3 > 1.1 \times \overline{O_3}$, 4: $^{7}Be > 8$, $RH < 40$, $O_3 > 1.2 \times \overline{O_3}$, 5: $^{7}Be > 8$, $RH < 30$, $O_3 > 1.2 \times \overline{O_3}$, 6: $^{7}Be > 8$, $RH < 20$, $O_3 > 1.2 \times \overline{O_3}$, 7: $^{7}Be > 10$, $RH < 30$, $O_3 > 1.1 \times \overline{O_3}$, 8: $^{7}Be > 6$, $RH < 30$, $O_3 > 1.1 \times \overline{O_3}$.

the frequency of intrusion days is plotted for different thresholds of the applied criteria. The absolute values deviate by up to more than a factor of three from our reference climatology (criterion 2 in Fig. 15). Consequently, absolute values for the frequency of stratospheric intrusions can only be derived with large, but not exactly quantified uncertainty. Most importantly, the shape of the annual cycle is stable against variations in the thresholds.

We have also studied the threshold sensitivity when using specific humidity instead of the RH criterion. If the specific humidity threshold is tuned to give the same annually averaged frequency of intrusions as the RH criterion, the two climatologies agree very well. A small systematic difference is a somewhat decreased intrusion frequency from July through September, and a somewhat increased frequency in November and December. This is caused by the higher specific humidity levels in the troposphere in summer than in winter.

5.2. Seasonal variation of stratospheric intrusions at mountain peaks

The average frequency of intrusions detected at Zugspitze during the period 1991 to 1997 is 5.5%, consistent with values reported by Scheel et al. (1999) for 1996 and 1997 only. Intrusions are most frequent in October (12%) with a secondary maximum in winter and early spring. A deep summer minimum ($<3\%$) during May through August is found (Fig. 16). Using the same selection criteria, the average intrusion frequency at Sonnblick (10%) is higher than that at Zugspitze. As at Zugspitze, intrusions are most frequent in October, and feature a secondary maximum in winter and a summer minimum. However, the seasonal variation is less systematic due to the smaller data set available for Sonnblick.

At Jungfraujoch, the average intrusion frequency (17%) is still higher than at Sonnblick. Also in contrast to the other stations, there is little seasonal variation. The high value for July should be interpreted with caution, since it is based on data from a single year, 1996 (for July 1997 ^{7}Be data were missing). One possible explanation for the differences to the other stations would be the coarser time resolution of the ^{7}Be data. However, using 48-h mean ^{7}Be concentrations at Zugspitze reduces the annual mean intrusion frequency from 5.5% to 3.6%, and has only small effects on the seasonal variation. Thus, the reason for the much higher frequency of intrusions and the missing seasonal variation at Jungfraujoch remains unclear at this time. A further discussion on this is given in Section 7.

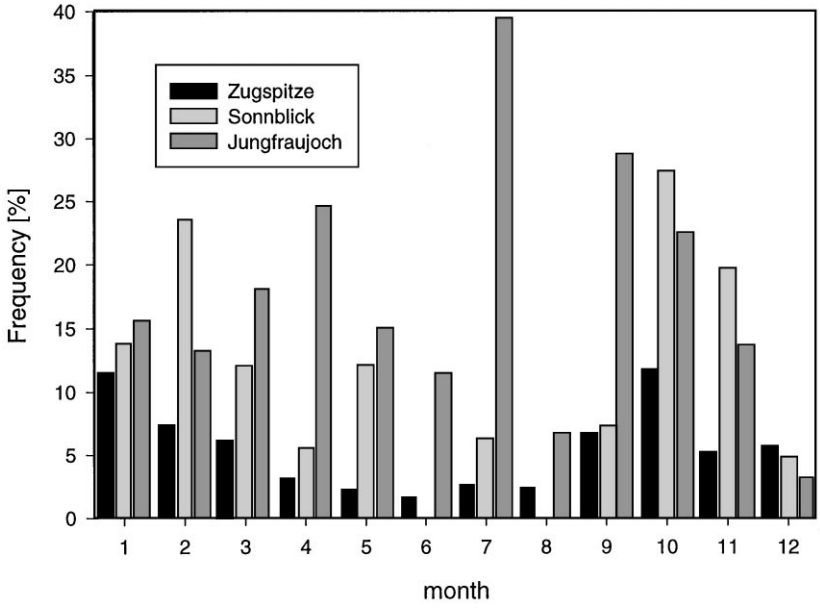

Fig. 16. Seasonal variation of the frequency of stratospheric intrusion days at the sites Zugspitze, Sonnblick and Jungfraujoch as obtained with the detection algorithm based on criterion 2 (Fig. 1).

6. Model validation on longer time-scales

For technical reasons we did not generate the full output for the three-year model runs, but calculated tracer mixing ratios only at certain receptor locations. These receptor locations were $1^\circ \times 1^\circ$ grid cells around the four mountain peaks, five $2^\circ \times 2^\circ$ grid cells covering the Alpine region, and a large "European" box covering the region 0° to 30°E and 40° to 60°N. In all grid cells, mixing ratios were determined in eight layers 500 m high from 0 to 4000 m asl. In the following we report the tracer mixing ratios for Mt. Cimone in the fifth layer, for Zugspitze in the sixth layer, for Sonnblick in the seventh layer, and for Jungfraujoch in the eighth layer.

Due to many contributing factors, the relationship between transport from the stratosphere and observations of O_3 and ^{7}Be is not so simple that correlation analyses between modeled tracer mixing ratios and measurement data would yield meaningful results. The respective correlation coefficients were not significantly different from zero for both ^{7}Be and O_3. Therefore, we developed a different method to validate our results. For all days with the daily mean O_3 tracer mixing ratio exceeding a certain threshold (i.e., "model intrusion days"), we determined a daily mean measured value C_M (of either ^{7}Be, O_3 or RH) and a baseline value C_B. C_B is the average of all daily means of measured values that were available within a 60-day period centered at the intrusion day and for which the model predicted less than 1 ppb O_3 tracer. It thus represents an expectation value in the hypothetical absence of the intrusion. We expect $C_M > C_B$ for ^{7}Be and O_3, and $C_M < C_B$ for RH.

Table 2 reports the average deviation $\overline{\Delta C} = 1/N \sum_{i=1}^{N}(C_{M_i} - C_{B_i})$, where N is the number of cases with daily mean stratospheric O_3 tracer mixing ratios above 20 ppb. The threshold of 20 ppb was chosen because it selects 3 to 7% (depending on station and periods with available data) of all days, which is roughly the frequency of stratospheric intrusions identified in the measurement data. Concentrations of ^{7}Be on simulated intrusion days are, on average, clearly above the baseline values. At Zugspitze, for instance, the $\overline{\Delta C}$ of 2.7 mBq m^{-3} for all intrusions and 4.7 mBq m^{-3} for intrusions aged less than four days are in the same range as the mean ^{7}Be deviation (4.2 mBq m^{-3}) found by Elbern et al. (1997) for intrusion days identified from measurement data. Student's t test (Press et al., 1990) showed that the averages of C_M and C_B are significantly different from each other for both Zugspitze and Sonnblick. Thus, the model generally seems to identify intrusion episodes correctly, although the large standard deviations indicate considerable scatter. Indeed, there are a few cases with $C_B > C_M$. This may either be due to removal of ^{7}Be by precipitation, or erroneous model simulations for these days. At Jungfraujoch, the results are insignificant, which can be explained partly by the longer ^{7}Be sampling interval at that station.

$\overline{\Delta C}$ for RH is (at most stations significantly) negative, confirming the expected humidity drop on intrusion days, but again the standard deviations are large. The

Table 2
Average deviation $\overline{\Delta C}$ of the measured values from the baseline values of ^{7}Be, RH and ozone at the mountain peak stations (see text for explanation) for an ozone tracer threshold value of 20 ppb. The results for intrusions aged less than four days and for all intrusions together are shown separately. Values in brackets are standard deviations. One (two) asterisks denote values that are significant on the 90% (95%) confidence level. $\overline{\Delta C}$ was calculated using all measurement data available for the period January 1995 to January 1998 (see Table 1)

Receptor	^{7}Be (mBq m^{-3})		RH (%)		Ozone (ppb)	
	Age < 4	Total	Age < 4	Total	Age < 4	Total
Mt. Cimone	—	—	− 21.4** (15.4)	− 8.7 (18.9)	6.3 (4.8)	3.9 (4.2)
Zugspitze	4.8** (6.3)	2.8** (5.2)	− 21.9** (26.7)	− 13.6** (26.8)	3.3 (6.4)	3.1* (6.2)
Sonnblick	6.8** (8.0)	5.8** (7.2)	− 12.2 (21.0)	− 10.7** (24.1)	6.8** (6.8)	4.7** (6.5)
Jungfraujoch	3.2 (5.1)	4.1 (7.0)	− 19.3** (22.5)	− 16.0** (23.2)	4.8** (5.5)	4.3** (5.6)

Table 3
Average simulated O_3 tracer mixing ratios (ppb) for intrusion days and non-intrusion days as found in the observational climatology. The results for intrusions aged less than four days and for all intrusions together are shown separately. Values in brackets are standard deviations. The comparison was done for the period January 1995 to January 1998, given that observations of ^{7}Be, O_3 and RH were simultaneously available (compare Table 1). Asterisks in the intrusion days columns show that the tracer mixing ratios are on the 95% confidence level significantly higher than on non-intrusion days

Receptor	Intrusion days		Non-intrusion days	
	Age < 4	Total	Age < 4	Total
Zugspitze	6.6* (18.5)	11.7* (19.9)	0.9 (3.3)	4.2 (11.5)
Sonnblick	5.8* (13.0)	9.7* (14.6)	1.7 (7.0)	4.7 (9.6)
Jungfraujoch	3.0 (6.4)	8.1 (14.1)	2.4 (6.0)	5.8 (8.9)

data also show that intrusions with a tropospheric age of less than four days correspond better with the humidity data than older ones. $\overline{C}$ for O_3 is positive, but the surplus is only a few ppb.

For a direct comparison between the observational and the model climatology, Table 3 shows the average O_3 tracer mixing ratios on days flagged as "intrusion days" in the observational climatology and those on the other days. Average O_3 tracer mixing ratios are higher by a factor of three and a factor of two at Zugspitze and Sonnblick, respectively, on intrusion days than on non-intrusion days. These differences are even larger for tracer of age less than four days (factors of seven and four). According to Student's *t*-test (Press et al., 1990), all these differences are significant at the 95% level. At Jungfraujoch the difference between intrusion days and non-intrusion days is smaller and not significant at the 95% confidence level, partly because the detection algorithm is coarser due to the 48 h time resolution of the ^{7}Be data.

6.1. Three-year model climatology

6.1.1. Average mixing ratios, interannual variability and frequency distributions

Based on the model results, the average O_3 (stratospheric air) tracer mixing ratios during the period January 1995 to September 1997 are 4.2, 4.5, 5.6 and 7.1 ppb (1.8, 1.8, 2.2, 2.5%) for Mt. Cimone, Zugspitze, Sonnblick and Jungfraujoch, respectively (Table 4). The variation between the stations largely reflects the effect of altitude, as evidenced by Fig. 17, which shows the vertical distribution of the average O_3 tracer mixing ratios in the European box resulting from stratospheric intrusions of different age classes. The average tracer mixing ratios for the uppermost four levels largely correspond to those at the mountain stations, which are, however, slightly modified due to geographical differences. While there is a significant contribution of direct intrusions to the O_3 mixing ratios at the altitudes of the mountain peaks, their influence in the lowlands is obviously much smaller (Fig. 17). The influence on boundary-layer O_3 concentrations should be seen in comparison to the fast photochemical processes in the continental boundary layer, which probably dominate the O_3 budget.

For intrusions aged less than one day, there is no uniform increase in O_3 tracer mixing ratios with height (Fig. 17). Calculations yield a minimum in the layer from 2000–2500 m, below which the mixing ratios increase with decreasing altitude. This may be explained by the fast descent of these intrusions, which cross higher levels very fast and cause only short spikes in the O_3 tracer (see also Eisele et al., 1999). Closer to the surface, their descent comes to a stop, and the O_3 tracer peaks become broader.

Approximately 30–50% of the total mixing ratios simulated are due to stratospheric air aged less than four

Table 4
Average stratospheric ozone tracer mixing ratios (ppb) in the years 1995, 1996 and 1997 and for the whole period for stratospheric air aged less than four days and for all cases

	Age < 4 days				All ages			
Receptor	1995	1996	1997	1995–1997	1995	1996	1997	1995–1997
Mt. Cimone	1.5	0.7	1.6	1.3	4.3	4.0	4.3	4.2
Zugspitze	1.4	1.2	1.6	1.4	3.6	5.5	4.4	4.5
Sonnblick	2.1	1.9	2.0	2.0	4.3	7.6	5.0	5.6
Jungfraujoch	4.8	3.2	2.2	3.5	7.5	8.4	5.3	7.1
Europe, layer 8	3.8	3.7	3.7	3.7	7.2	9.2	7.9	8.1
Europe, layer 1	0.8	0.7	0.7	0.7	2.0	2.0	2.0	2.0

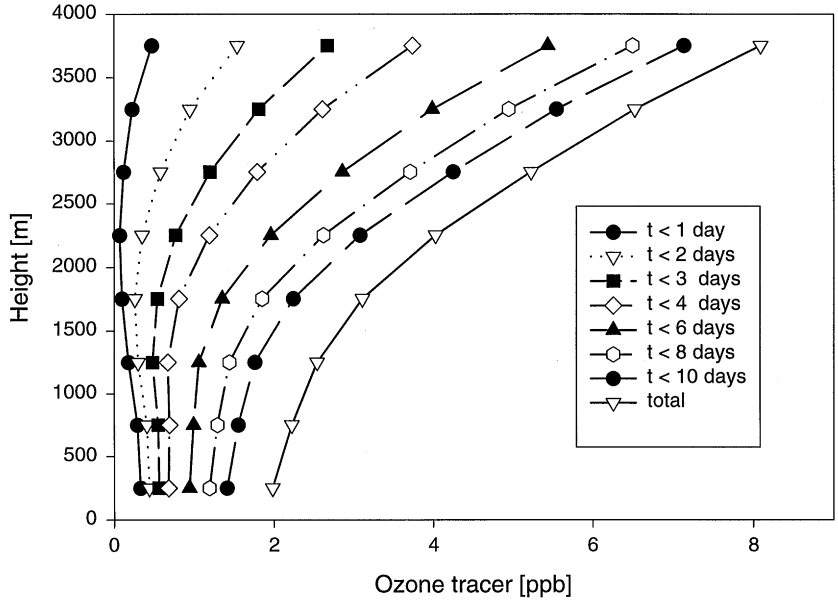

Fig. 17. Vertical profiles of the calculated average O_3 tracer mixing ratios in the European box for eight different age classes.

days. Note that the total mixing ratios depend on the size of the model domain, while the "fresh" intrusions are almost fully captured with our limited domain. There is also considerable interannual variation in the O_3 tracer mixing ratios at individual stations (Table 4). For instance, average tracer mixing ratios of age less than four days at Jungfraujoch were 4.8 ppb in the year 1995, but only 2.2 ppb in 1997. For the larger European box, however, the interannual variability is very small.

Table 5 shows the frequency distributions of the 3-h mean O_3 tracer mixing ratios. At all stations, the model results show a nearly permanent, albeit low, stratospheric background. With a global model domain, this background would be present all the time. However, only during some 30% of the time, "fresh" stratospheric air aged less than four days is present. During 10–15% of the time, stratospheric O_3 tracer mixing ratios are higher than 10 ppb. With the exception of Jungfraujoch, less than 1% of the time do O_3 tracer mixing ratios exceed 80 ppb, and only half of these cases are "fresh" intrusions. The frequency of high tracer mixing ratios shows a strong vertical gradient. For instance, the frequency of "fresh" stratospheric O_3 mixing ratios above 80 ppb is 0.2, 0.3, 0.5 and 0.9% at Mt. Cimone, Zugspitze, Sonnblick and Jungfraujoch, respectively.

6.1.2. Seasonality

Fig. 18 shows the seasonal variation of the O_3 tracer, averaged over the three years, at the mountain peaks and in the highest and lowest layer of the "European" box.

Table 5
Frequency (%) of 3-h mean stratospheric ozone tracer mixing ratios greater than 0, 10, 20, 40, 60, 80 and 100 ppb at the four mountain peaks

Receptor	0 ppb	10 ppb	20 ppb	40 ppb	60 ppb	80 ppb	100 ppb
Mt. Cimone, age < 4 days	33.4	2.9	1.4	0.6	0.3	0.2	0.1
Mt. Cimone, all cases	81.5	10.2	3.7	1.3	0.6	0.3	0.2
Zugspitze, age < 4 days	32.3	3.0	1.6	0.7	0.4	0.3	0.1
Zugspitze, all cases	77.3	10.2	4.2	1.5	0.8	0.5	0.4
Sonnblick, age < 4 days	29.6	4.0	2.3	1.2	0.7	0.5	0.3
Sonnblick, all cases	73.7	12.3	5.5	2.3	1.3	1.0	0.7
Jungfraujoch, age < 4 days	31.4	6.2	3.7	1.9	1.2	0.9	0.7
Jungfraujoch, all cases	68.1	15.1	8.1	3.6	2.2	1.4	1.0

A strong seasonal variation is evident at all sites, with a minimum in mid-summer and a maximum in late winter/early spring. At the highest station, Jungfraujoch, the variation is weakest and a secondary October maximum appears.

An interesting result is the almost complete absence of direct intrusions with a tropospheric age of less than four days in mid-summer. Direct stratospheric intrusions deliver 4–25 times more O_3 tracer to our receptor boxes during February through April than during June through August (Table 6). This strong seasonal variation is only partly due to the initialization of the O_3 tracer in relation to PV. Mainly it is caused by differences in the circulation patterns of the atmosphere. For instance, not a single strong direct intrusion episode was simulated for the summers of 1995–1997 at Mt. Cimone, Sonnblick and Zugspitze.

Inspection of the results for the five $2^\circ \times 2^\circ$ grid cells arranged in west–east direction over the Alps revealed a strong west–east gradient in the seasonal variation of direct intrusions. In Table 6 this is shown for the sixth model level, but a similar gradient can be found at the other levels as well. In summer, intrusions aged less than four days are (by almost a factor of two) more frequent in the westernmost grid cell than in the easternmost one. The reason for this seems to be that major cyclonic disturbances do not regularly penetrate deep into the European continent in summer and stratospheric intrusions therefore rarely occur directly over Europe. In late winter/early spring, the opposite gradient is found; i.e., higher O_3 tracer concentrations (by more than a factor of 1.5) in the eastern Alps than in the western Alps. This is probably caused by a greater mesoscale influence of lee-cyclogenesis (see Buzzi et al., 1984) in the eastern than in the western Alps.

Although the calculated O_3 tracer concentrations represent only intrusions occurring in our model domain and are thus somewhat arbitrary, it was interesting to compare them with O_3 concentrations measured at the peak stations. In Fig. 19, we show their relative contribution to the measured O_3 concentrations (Fig. 19). Since the measured O_3 concentrations have a reverse seasonal variation as compared to the stratospheric tracer, the seasonal variation of the stratospheric contribution is increased. While in summer the average contribution to the total O_3 concentrations is only 3–5% (with the exception of Jungfraujoch, where it is almost 10%) counting all intrusions, and nearly zero counting only intrusions of age less than four days, there is a major contribution (on the order of 10–25%) in winter, with larger effects at the higher stations Sonnblick and Jungfraujoch. At Jungfraujoch, where the impact of intrusions aged less than four days is largest, they contribute 10–20% in autumn and late winter.

7. Discussion and conclusions

In this paper, we have first studied two episodes of stratospheric intrusions impinging on the Alpine area, one occurring in the spring, the other in the autumn of 1996. These two episodes were selected from a large number of intrusions studied by us during the last few years (e.g., Bonasoni et al., 1999; Stohl and Trickl, 1999; Eisele et al., 1999) and served as test cases for the FLEXPART model.

In the autumn episode, a folding of the tropopause and subsequent cut-off low formation led to the intrusion of stratospheric air into the troposphere. The intrusion first affected Jungfraujoch, half a day later Zugspitze, and after a few more hours also Sonnblick. This west–east drift of the stratospheric air was reproduced by the model. Maximum model-predicted stratospheric O_3 tracer mixing ratios were 35, 45 and 60 ppb at the three observatories (stratospheric air mixing ratios were 30–50%). The stronger intensity of the modeled intrusion in the eastern Alps was consistent with the ^{7}Be measurements. However, the maximum measured O_3 mixing ratios at all three high-Alpine observatories were remarkably similar, 72–73 ppb, while the duration of the

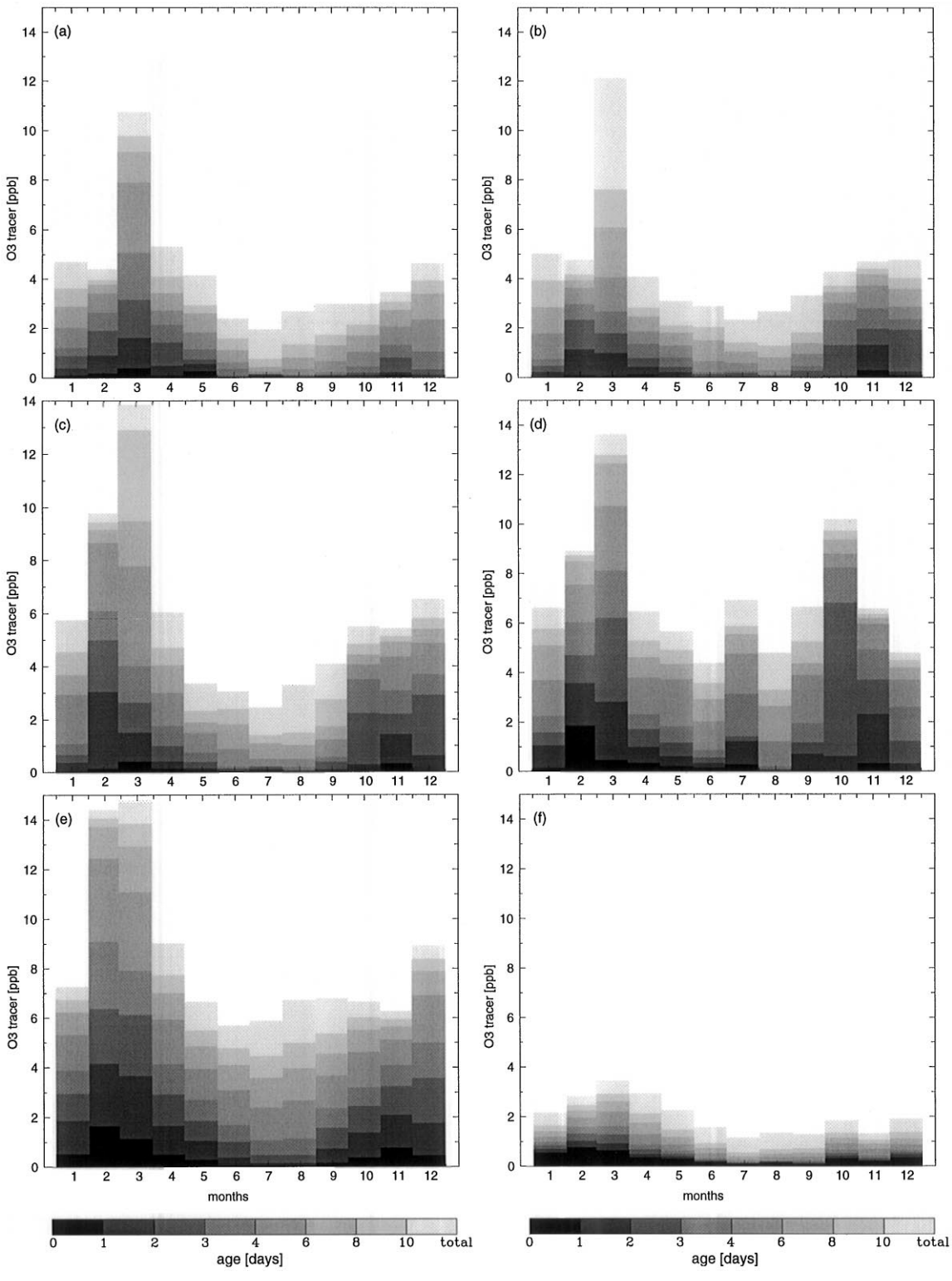

Fig. 18. Seasonal variation of the modeled ozone tracer mixing ratios at Mt. Cimone (a), Zugspitze (b), Sonnblick (c), Jungfraujoch (d), at 3500–4000 m in the European box (e), and at the surface in the European box (f).

Table 6
Average stratospheric ozone tracer mixing ratios due to direct intrusions having a tropospheric age of less than four days for winter/spring (February–April) and for summer (June–August), and the corresponding concentration ratio

Receptor	Winter/Spring (ppb)	Summer (ppb)	Ratio
Mt. Cimone	3.30	0.22	15
Zugspitze	2.31	0.20	12
Sonnblick	3.81	0.20	18
Jungfraujoch	5.45	1.39	4
Westernmost grid cell, layer 6	2.59	0.25	10
Easternmost grid cell, layer 6	4.00	0.16	25
Europe, layer 8	6.97	1.30	5
Europe, layer 1	1.36	0.24	6

O_3 peak was much shorter at Jungfraujoch than at the other two stations. Elevated O_3 concentrations and minima in RH were also reported from several sites at lower altitudes, with the signal becoming weaker with decreasing altitude.

Three stratospheric intrusions were found to influence O_3 concentrations in the Alps and Apennines during a ten-day period in spring 1996. The most intense one, caused by direct descent of stratospheric air above the Alps, first affected the Alpine peak stations (again proceeding from west to east) before it hit Mt. Cimone in the northern Apennines one day later. There it yielded very high ^{7}Be and O_3 concentrations and a drop of RH to the detection limit. Clear evidence exists that this intrusion also penetrated to the floor of several Alpine valleys.

Two more intrusions happened during this ten-day period, one before and one after the main intrusion. The region south of the Alps acted as a "shaker", where stratospheric air masses from all three intrusions mixed with each other and with the surrounding tropospheric air. The high O_3 concentrations observed in large areas in and south of the Alps during the period following the descent of the main intrusion were only to a small part directly caused by stratospheric O_3. Since the meteorological conditions supported photochemical O_3 formation and there was ample supply of precursors emitted in the Po Basin, a major part of the O_3 was most probably of photochemical origin. However, due to the strong mixing between stratospheric and tropospheric air the effects of photochemical O_3 formation and intrusions of stratospheric air cannot be distinguished. Since, in the presence of water vapor, photolysis of O_3 is the major source of hydroxyl (OH) radicals that are central to photochemical O_3 formation, the O_3 brought down in stratospheric intrusions can trigger photochemical processes given sufficiently high concentrations of nitrogen oxides and hydrocarbons. This may be of special importance at the beginning of photochemical episodes, when otherwise low O_3 concentrations limit the supply with OH to "burn" the hydrocarbons. There are first indications that the proposed mechanism is on principle correct. Preliminary simulations of the spring episode with the EURAD chemistry transport model (Feldmann et al., 1999) show high OH concentrations especially in the mixing region between the stratospheric and the tropospheric air. Such a mechanism may also contribute to the spring-time O_3 maximum observed in many remote areas.

An important conclusion of the case studies is that the passive Lagrangian tracer model used here is a suitable diagnostic tool for studying stratospheric intrusions. Excellent agreement was found between the modeled intrusion of stratospheric air and water vapor satellite images. This indicates that the main transport mechanisms in the lower stratosphere and upper troposphere were well captured by the ECMWF analyses. There was also good overall agreement with observations at Alpine peaks. For the first episode, observed O_3 mixing ratios could be explained quantitatively by the model results. For the second episode, the impact of the intrusion on the mountain peaks was underestimated. However, this was due to a displacement of the intrusion by approximately 200 km and not to a systematic underprediction. In additional case studies, not presented in this paper, a similar model performance was obtained.

Moreover, we have presented two independent short climatologies of O_3 transported down to high-Alpine sites during intrusions of stratospheric air. The first one is based entirely on measurement data at three mountain summits and yields the frequency of stratospheric intrusions at these sites without explicitly calculating their impact on O_3 levels. The second one results from a three-year tracer model simulation and gives average mixing ratios of both an O_3 and an air tracer originating in the stratosphere. There is significant agreement between the two methods for two of the three stations (Sonnblick, Zugspitze) even if individual events are directly compared. O_3 tracer mixing ratios resulting from modeled intrusions of tropospheric age less than four days at Zugspitze and Sonnblick are seven and four times higher on days flagged as "intrusion days" by the measurement data screening algorithm than on "non-intrusion days". For Jungfraujoch, the agreement is less good, which is partly related to the coarser time resolution (48 h) of the ^{7}Be measurements at this site, and partly also to other factors (see below).

The frequency of stratospheric intrusions identified from the measurements at Sonnblick and Zugspitze shows a deep summer minimum. This is confirmed by the model results, where direct intrusions of age less than

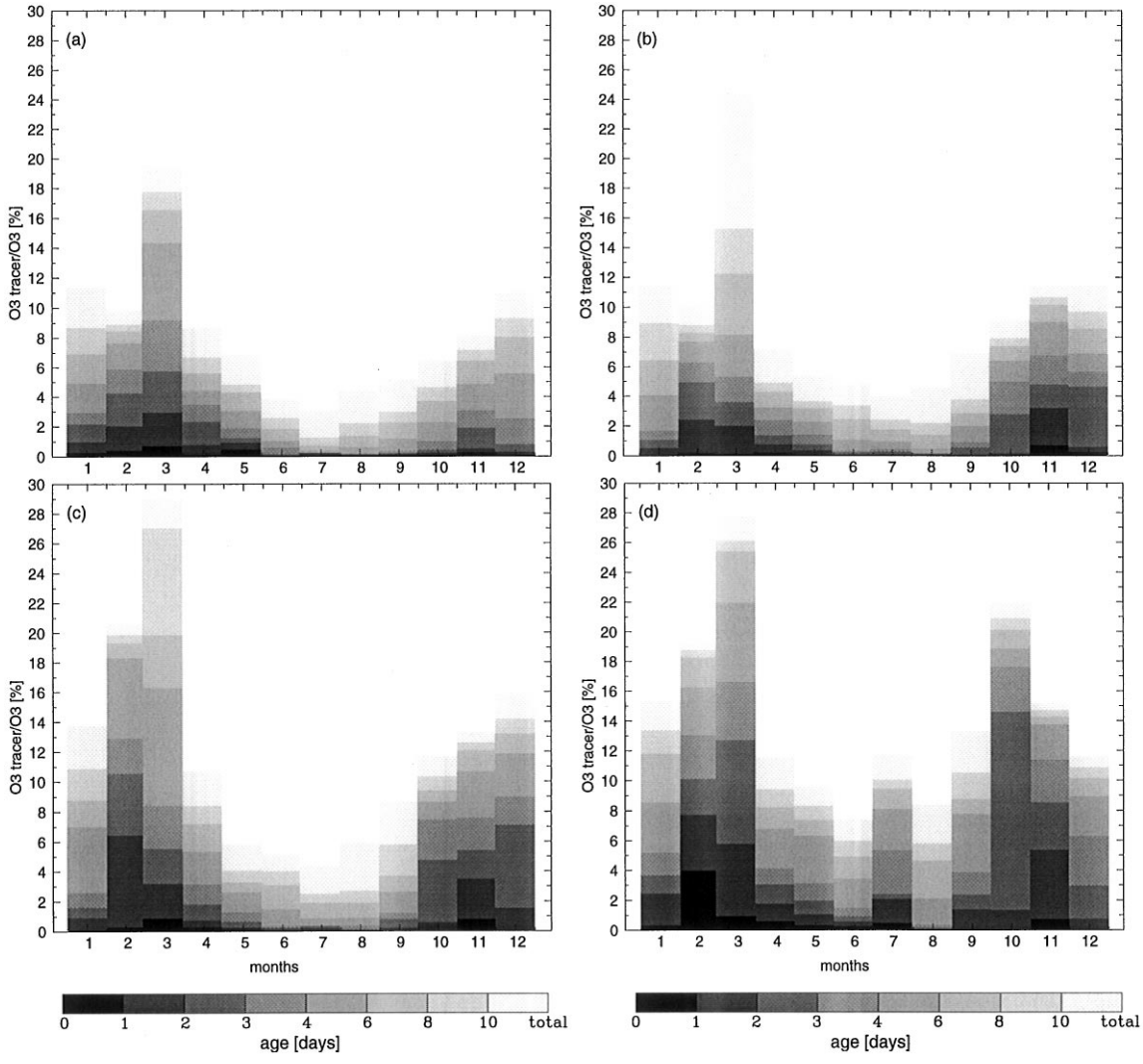

Fig. 19. Seasonal variation of the relative contribution of the ozone tracer to the total measured mixing ratios at Mt. Cimone (a), Zugspitze (b), Sonnblick (c) and Jungfraujoch (d).

four days are completely absent in summer. The modeled seasonal variation shows a late-winter/early-spring maximum in average O_3 tracer mixing ratios, whereas the observations reveal an early-autumn maximum and a secondary January/February maximum in the frequency of stratospheric intrusions. This discrepancy is practically removed when the stratospheric air tracer instead of the O_3 tracer is considered: for direct intrusions with a tropospheric age of less than four days, monthly average stratospheric air tracer mixing ratios at the Zugspitze summit are highest in November at 1.5% and exhibit a secondary maximum in February at 1.2%. The reason for the differences between the O_3 tracer and the stratospheric air tracer lies in the initialization of O_3 in the stratosphere, which is highest in spring and lowest in autumn.

Our observational climatology, with a summer minimum and an autumn maximum of stratospheric intrusions confirms results by Scheel et al. (1999) obtained from an analysis of Zugspitze data from 1997. The summer minimum was also found by Elbern et al. (1997) for a 10-yr data set from Zugspitze, but the seasonal variation was much smaller than the one derived here. The reason for this may be that Elbern et al. (1997) required ^{7}Be concentrations to exceed the running monthly means by more than two standard deviations during an intrusion. This automatically fixes a certain number of cases in each month for pure statistical reasons and smoothes the

seasonal variation. Furthermore, they did not use RH as a criterion.

The observations at Jungfraujoch show no clear seasonal variation, but stratospheric intrusions occur more frequently than at the other stations almost throughout the year. The model results agree with the seasonal variation only insofar as the summer minimum in average O_3 tracer mixing ratios is less deep than at the other stations. However, the disagreement is reduced when the different periods of the climatologies are considered. The observational climatology does not cover the year 1995, for which the model results showed a much deeper summer minimum than for the following years. Furthermore, the high frequency in July is based only on measurements during the year 1996, when the model results also showed the largest intrusion activity.

The average observed intrusion frequencies at Zugspitze, Sonnblick and Jungfraujoch are 5.5%, 10% and 17%, respectively. If only the period for which data from Jungfraujoch are available are used for the Zugspitze climatology, the intrusion frequency increases to 7% and the difference between the stations is somewhat smaller. Although a higher frequency may be expected for Jungfraujoch, the highest station, than for Zugspitze, the lowest one, the large differences can hardly be explained by the different altitudes alone. For instance, most of the intrusions identified by Eisele et al. (1999) in the free troposphere with lidar measurements also reached the Zugspitze site. The differences are also not supported by the model results, which show much smaller deviations between the stations. At present, the reason for the high frequency of observed intrusions at Jungfraujoch remains unclear. Possibly the detection algorithm, which was set up by studying intrusions mostly for Zugspitze, is less suited for Jungfraujoch. At that altitude, tropospheric air may more often show signatures (low RH, high ^{7}Be concentrations) that at lower levels are characteristic for stratospheric intrusions. Thus, for Jungfraujoch a higher threshold level for ^{7}Be and a lower one for RH would probably be more adequate. In any case, more measurements at Sonnblick and Jungfraujoch are needed to establish stable climatologies.

The seasonal variation of modeled O_3 tracer mixing ratios at all three stations is strikingly similar to the seasonal variation in the frequency of tropopause folds identified from ozone soundings at a number of European sites by Blonsky and Speth (1998). In their Fig. 3, they show an increase in the frequency of folds from January through March, followed by a steep drop in April. Van Haver et al. (1996), in a similar study of tropopause folds, found little seasonal variation, but noted that O_3 concentrations within the folds were largest in spring. A summer minimum in the frequency and intensity of tropopause folds was also detected by Elbern et al. (1998) using Q-vector diagnostics applied to global ECMWF analyses. Our seasonal variation of O_3 tracer mixing ratios is similar to the variation of the downward flow across the 100 hPa surface, which exhibits a winter maximum and summer minimum (e.g., Holton, 1990; van Velthoven and Kelder, 1996). It is, however, not fully consistent with the seasonal variation of the mass flux across the tropopause obtained by Appenzeller et al. (1996b). From global-scale considerations they found a late-spring maximum and an early-autumn minimum in northern hemispheric mass flux across the tropopause.

The model results show a clear vertical gradient in the O_3 tracer mixing ratios. Mixing ratios in the "European" box between the surface and 500 m asl are lower by a factor four than those between 3500 and 4000 m asl. According to the model results, the seasonal variation of direct stratospheric intrusions is stronger (by a factor of 2.5) in the eastern than in the western Alps, although the annual average tracer mixing ratios are similar for the same altitude in both regions. This feature was found for each individual year of the climatology and is probably caused by the flow patterns specific to central Europe and the Alpine region. The deeper summer minimum in the east may be caused by blocking of major cyclonic disturbances from penetrating far into the European continent in summer, whereas the larger winter/spring maximum in the east may be related to lee-cyclogenesis south of the Alps. The fact that such distinct differences occur over a relatively short distance (approximately 500 km) also shows that the climatology is very specific to the Alpine region and should not be generalized. Differences in the average tropospheric O_3 content over similar scales were also reported by Beekmann et al. (1994) in a comparison of data from several ozone sounding sites in western Europe and were attributed to possible differences in STE.

From our results it appears that stratospheric O_3 is of limited, but not negligible significance for the ozone budget of the boundary layer. The case studies showed that stratospheric intrusions can occasionally penetrate directly down to the surface and yield a signature in the O_3 mixing ratios; but these are rare events. Accordingly, in our model climatology the lowest layer receives only a few ppb of stratospheric O_3. However, this influence may be much higher if aged intrusions, which are not covered by our model domain, actually play an important role.

The model results presented here clearly indicate that stratospheric intrusions are of great importance for the O_3 budget of the lower free troposphere, at least over central Europe, and especially in late winter/early spring. During that season stratospheric intrusions occurring within our limited domain contribute about 15–25% to the O_3 concentrations measured at high Alpine peaks. Much of the stratospheric O_3 arrives at the stations strongly diluted by mixture with tropospheric air and is thus sometimes not recognizable as stratospheric O_3 by the measurements.

How important stratospheric intrusions really are for tropospheric chemistry critically depends on the lifetime of O_3. Its lifetime in the winter, when STE is most active is estimated to be on the order of a month (Fishman et al., 1979). However, even for a relatively short tropospheric lifetime of about one week, our model results suggest that stratospheric intrusions are a very important factor for the tropospheric O_3 budget. These results are in clear contrast to the model studies of Austin and Follows (1991) and Follows and Austin (1992) who found that stratospheric O_3 contributes less than 5% at the surface and less than 10% at 700 hPa throughout the year.

Our results are in much better agreement with the model studies of Roelofs and Lelieveld (1997) and Roelofs et al. (1997), who found that the stratosphere contributes 40% of the tropospheric O_3. Over Europe and at the altitude of our peak stations, this contribution may be even higher in winter/spring if intrusions from outside our model domain are accounted for. Further studies with an extended model domain are planned to answer this question.

Acknowledgements

This study was part of the EU research project "Vertical ozone transports in the Alps (VOTALP)", funded by the European Commission under Framework Programme IV, Environment and Climate, contract number ENV4-CT95-0025, and by the governments of Switzerland and Austria. The authors are grateful to all colleagues involved in the measurements or in the processing of data for the project and to the whole VOTALP community for stimulating discussions. ECMWF and Deutscher Wetterdienst kindly admitted access to ECMWF data within the special project "Validation of trajectory calculations". Ozone sounding and ground level data from Hohenpeißenberg were made available by W. Fricke and H. Claude from Deutscher Wetterdienst, TOVS data were prepared by NCEP and downloaded from http://auc.dfd.dlr.de/info/AUC/index.html. The Swiss Meteorological Institute provided ozone sounding data from Payerne and meteorological data from Jungfraujoch via the Paul Scherrer Institute. S. Simic supplied us with total column ozone measurements from Sonnblick (funded by the Austrian Ministry of the Environment). Further data were provided by the Umweltbundesamt (Austria), the Amt der Salzburger Landesregierung (Austria), the Bundesamt für Umwelt, Wald und Landwirtschaft (Switzerland), the Landesagentur für Umwelt- und Arbeitsschutz and the Autonome Provinz Bozen Südtirol (Italy). We thank P. Fabian, R. Meyer and H. Wernli for their comments on a previous version of this paper, and two constructive anonymous reviews helped to generate the final version.

References

Ancellet, G., Beekman, M., Papayannis, A., 1994. Impact of a cutoff low development on downward transport of ozone in the troposphere. Journal of Geophysical Research 99, 3451–3468.

Appenzeller, C., Davies, H.C., 1992. Stucture of stratospheric intrusions into the troposphere. Nature 358, 570–572.

Appenzeller, C., Davies, H.C., Norton, W.A., 1996a. Fragmentation of stratospheric intrusions. Journal of Geophysical Research 101, 1435–1456.

Appenzeller, C., Holton, J.R., Rosenlof, K.H., 1996b. Seasonal variation of mass transport across the tropopause. Journal of Geophysical Research 101, 15071–15078.

Austin, J.F., Follows, M.J., 1991. The ozone record at Payerne: an assessment of the cross-tropopause flux. Atmospheric Environment 25A, 1873–1880.

Bachmeier, A.S., Shipham, M.C., Browell, E.V., Grant, W.B., Klassa, J.M., 1994. Stratospheric/tropospheric exchange affecting the northern wetlands regions of Canada during summer 1990. Journal of Geophysical Research 99, 1793–1804.

Baskaran, M., 1995. A search for the seasonal variability on the depositional fluxes of ^{7}Be and ^{210}Pb. Journal of Geophysical Research 100, 2833–2840.

Baumann, K., Stohl, A., 1997. Validation of a long-range trajectory model using gas balloon tracks from the Gordon Bennett Cup 95. Journal of Applied Meteorology 36, 711–720.

Beekmann, M., Ancellet, G., Blonsky, S., De Muer, D., Ebel, A., Elbern, H., Hendricks, J., Kowol, J., Mancier, C., Sladkovic, R., Smit, H.G.J., Speth, P., Trickl, T., Van Haver, Ph., 1997. Regional and global tropopause fold occurrence and related ozone flux across the tropopause. Journal of Atmospheric Chemistry 28, 29–44.

Beekmann, M., Ancellet, G., Mégie, G., 1994. Climatology of tropospheric ozone in southern Europe and its relation to potential vorticity. Journal of Geophysical Research 99, 12841–12853.

Bethan, S., Vaughan, G., Reid, S.J., 1996. A comparison of ozone and thermal tropopause heights and the impact of tropopause definition on quantifying the ozone content of the troposphere. Quarterly Journal of the Royal Meteorological Society 122, 929–944.

Blonsky, S., Speth, P., 1998. An algorithm to detect tropopause folds from ozone soundings. Meteorologische Zeitschrift N.F. 7, 153–162.

Bonasoni, P., Evangelisti, F., Bonafe', U., Ravegnani, F., Calzolari, F., Stohl, A., Tositti, L., Tubertini, O., Colombo, T., 1999. Stratospheric ozone intrusion episodes recorded at Mt. Cimone during the VOTALP project: case studies. Atmospheric Environment 34, 1355–1365.

Buzzi, A., Giovanelli, G., Nanni, T., Tagliazucca, M., 1984. Study of high ozone concentrations in the troposphere associated with lee cyclogenesis during ALPEX. Contributions to Atmospheric Physics 57, 380–392.

Chen, P., 1995. Isentropic cross-tropopause mass exchange in the extratropics. Journal of Geophysical Research 100, 16661–16673.

Danielsen, E.F., 1968. Stratospheric–tropospheric exchange based on radioactivity, ozone and potential vorticity. Journal of Atmospheric Science 25, 502–518.

Davies, T.D., Schuepbach, E., 1994. Episodes of high ozone concentrations at the surface resulting from transport down from the upper troposphere/lower stratosphere: a review and case studies. Atmospheric Environment 28, 53–68.

Derwent, R.G., Simmonds, P.G., Seuring, S., Dimmer, C., 1998. Observation and interpretation of the seasonal cycles in the surface concentrations of ozone and carbon monoxide at Mace Head, Ireland from 1990 to 1994. Atmospheric Environment 32, 145–157.

Dibb, J.E., Mecker, L.D., Finkel, R.C., Southon, J.R., Caffee, M.W., Barrie, L.A., 1994. Estimation of the stratospheric input to the Arctic troposphere: ^{7}Be and ^{10}Be in aerosols at Alert, Canada. Journal of Geophysical Research 99, 12855–12864.

Dutkiewicz, V.A., Husain, L., 1985. Stratospheric and tropospheric components of ^{7}Be in surface air. Journal of Geophysical Research 90, 5783–5788.

Ebel, A., Hass, H., Jakobs, H.J., Laube, M., Memmesheimer, M., Oberreuter, A., Geiss, H., Kuo, Y.-H., 1991. Simulation of ozone intrusion caused by a tropopause fold and cut-off low. Atmospheric Environment 25A, 2131–2144.

ECMWF, 1995. User Guide to ECMWF Products 2.1. Meteorological Bulletin M3.2. ECMWF, Reading, UK.

Eisele, H., Scheel, H.E., Sladkovic, R., Trickl, T., 1999. High-resolution lidar measurements of stratosphere–troposphere exchange. Journal of Atmospheric Science 56, 319–330.

Elbern, H., Hendricks, J., Ebel, A., 1998. A climatology of tropopause folds by global analyses. Theory in Applied Climatology 59, 181–200.

Elbern, H., Kowol, J., Sládkovic, R., Ebel, A., 1997. Deep stratospheric intrusions: a statistical assessment with model guided analyses. Atmospheric Environment 31, 3207–3226.

Fabian, P., Pruchniewicz, P.G., 1977. Meridional distribution of ozone in the troposphere and its seasonal variation. Journal of Geophysical Research 82, 2063–2073.

Feldmann, H., Memmesheimer, M., Ebel, A., Seibert, P., Wotawa, G., Kromp-Kolb, H., Trickl, T., Prevot, A., 1999. Evaluation of a regional-scale model for the alpine region with data from the VOTALP project. In: Borrell, P.M., Borrell, P. (Eds.), Proceedings of EUROTRAC-2 Symposium 98. WIT press, Southampton, p. 478–482.

Fischer, H., Eigenwillig, N., Müller, H., 1982. Information content of METEOSAT and Nimbus/THIR water vapor channel data: altitude association of observed phenomena. Journal of Applied Meteorology 20, 1344–1352.

Fishman, J., Solomon, S., Crutzen, P.J., 1979. Observational and theoretical evidence in support of a significant in-situ photochemical source of tropospheric ozone. Tellus 31, 432–446.

Follows, M.J., Austin, J.F., 1992. A zonal average model of the stratospheric contributions to the tropospheric ozone budget. Journal of Geophysical Research 97, 18047–18060.

Hanna, S.R., 1982. Applications in air pollution modeling. In: Nieuwstadt, F.T.M., van Dop, H. (Eds.), Atmospheric Turbulence and Air Pollution Modelling. D. Reidel Publishing Company, Dordrecht, Holland.

Haynes, P.H., Marks, C.J., McIntyre, M.E., Shepherd, T.G., Shine, K.P., 1991. On the "Downward Control" of extratropical diabatic circulations by eddy-induced mean zonal forces. Journal of Atmospheric Science 48, 651–678.

Hoerling, M.P., Schaack, T.K., Lenzen, A.J., 1991. Global objective tropopause analysis. Monthly Weather Review 119, 1816–1831.

Hoinka, K.P., 1997. The tropopause: discovery, definition and demarcation. Meteorologisches Zeitschrift N.F. 6, 281–303.

Holton, J.R., 1990. On the global exchange of mass between the stratosphere and troposphere. Journal Atmospheric Science 47, 392–395.

Holton, J.R., Haynes, P.H., McIntyre, E.M., Douglass, A.R., Rood, R.B., Pfister, L., 1995. Stratosphere–troposphere exchange. Reviews of Geophysics 33, 403–439.

Koch, D.M., Jacob, D.J., Graustein, W.C., 1996. Vertical transport of tropospheric aerosols as indicated by ^{7}Be and ^{210}Pb in a chemical tracer model. Journal of Geophysical Research 101, 18651–18666.

Koch, D.M., Mann, M.E., 1996. Spatial and temporal variability of ^{7}Be surface concentrations. Tellus 48B, 387–396.

Lamarque, J.-F., Hess, P.G., 1994. Cross-tropopause mass exchange and potential vorticity budget in a simulated tropopause folding. Journal of Atmospheric Science 51, 2246–2269.

Lamarque, J.-F., Langford, A.O., Proffitt, M.H., 1996. Cross-tropopause mixing of ozone through gravity wave breaking: observation and modeling. Journal of Geophysical Research 101, 22969–22976.

Levy, H., Mahlmann, J.D., Moxim, W.J., Liu, S.C., 1985. Tropospheric ozone: the role of transport. Journal of Geophysical Research 90, 3753–3772.

Lisac, I., Marki, A., Tiljak, D., Klasinc, L., Cvitaš, T., 1993. Stratospheric ozone intrusion over Zagreb, Croatia, on February 6, 1990. Meteorologische Zeitschrift N.F. 2, 224–231.

Liu, S.C., Trainer, M., Fehsenfeld, F.C., Parrish, D.D., Williams, E.J., Fahey, D.W., Hubler, G., Murphy, P.C., 1987. Ozone production in the rural troposphere and the implications for regional and global ozone distributions. Journal of Geophysical Research 92, 4191–4207.

Mahlmann, J.D., 1997. Dynamics of transport processes in the upper troposphere. Science 276, 1079–1083.

Mauzerall, D.L., Jacob, D.J., Fan, S.-M., Bradshaw, J.D., Gregory, G.L., Sachse, G.W., Blake, D.R., 1996. Origin of tropospheric ozone at remote high northern latitudes in summer. Journal of Geophysical Research 101, 4175–4188.

Mote, P.W., Rosenlof, K.H., McIntyre, M.E., Carr, E.S., Gille, J.C., Holton, J.R., Kinnersley, J.S., Pumphrey, H.C., Russell, J.M., Waters, J.W., 1996. An atmospheric tape recorder: the imprint of tropical tropopause temperatures on stratospheric water vapor. Journal of Geophysical Research 101, 3989–4006.

Murphy, D.M., Fahey, D.W., 1994. An estimate of the flux of stratospheric reactive nitrogen and ozone into the troposphere. Journal of Geophysical Research 99, 5325–5332.

Norton, W.A., 1994. Breaking Rossby waves in a model stratosphere diagnosed by a vortex-following coordinate system and a technique for advecting material contours. Journal of Atmospheric Science 51, 654–673.

Parrish, D.D., Trainer, M., Holloway, J.S., Yee, J.E., Warshawsky, M.S., Fehsenfeld, F.C., Forbes, G.L., Moody, J.L., 1998. Relationships between ozone and carbon monoxide at surface sites in the North Atlantic region. Journal of Geophysical Research 103, 13357–13376.

Plumb, R.A., 1996. A "tropical pipe" model of stratospheric transport. Journal of Geophysical Research 101, 3957–3972.

Poulida, O., Dickerson, R.R., Heymsfield, A., 1996. Stratosphere–troposphere exchange in a midlatitude mesoscale

convective complex. 1–Observations. Journal of Geophysical Research 101, 6823–6836.

Press, W.H., Flannery, B.P., Teukolsky, S.A., Vetterling, W.T., 1990. Numerical Recipes in FORTRAN. The Art of Scientific Computing. Cambridge University Press, New York, 702 pp.

Reiter, R., 1991. On the mean daily and seasonal variations of the vertical ozone profiles in the lower troposphere. Atmospheric Environment 25A, 1751–1757.

Reiter, R., Munzert, K., Kanter, H.-J., Pötzl, K., 1983. Cosmogenic radionuclides and ozone at a mountain station at 3.0 km a.s.l. Archiv fur Meteorologie, Geophysik und Bioklimatologie, Serie B 32, 131–160.

Roelofs, G.-J., Lelieveld, J., 1997. Model study of the influence of cross-tropopause O_3 transports on tropospheric O_3 levels. Tellus 49B, 38–55.

Roelofs, G.-J., Lelieveld, J., van Dorland, R., 1997. A three-dimensional chemistry/general circulation model simulation of anthropogenically derived ozone in the troposphere and its radiative forcing. Journal of Geophysical Research 102, 23389–23401.

Scheel, Sladkovic, R., Kanter, H.-J., 1999. Ozone variations at the Zugspitze (2962 m a.s.l.) during 1996–1997. In: Borrell, P.M., Borrell, P. (Eds.), Proceedings of EUROTRAC-2 Symposium 98. WIT press, Southampton, p. 260–263.

Scheele, M.P., Siegmund, P.C., Velthoven, P.F.J., 1996. Sensitivity of trajectories to data resolution and its dependence on the starting point: in or outside a tropopause fold. Meteorological Applications 3, 267–273.

Stohl, A., 1998a. The FLEXPART Particle Dispersion Model, Version 3.0. Model documentation available from URL http://www.forst.uni-muenchen.de/LST/METEOR/stohl/flexpart.html.

Stohl, A., 1998b. Computation, accuracy and applications of trajectories – a review and bibliography. Atmospheric Environment 32, 947–966.

Stohl, A., Hittenberger, M., Wotawa, G., 1998. Validation of the Lagrangian particle dispersion model FLEXPART against large scale tracer experiment data. Atmospheric Environment 24, 4245–4264.

Stohl, A., Seibert, P., 1998. Accuracy of trajectories as determined from the conservation of meteorological tracers. Quarterly Journal of the Royal Meteorological Society 125, 1465–1484.

Stohl, A., Thomson, D.J., 1999. A density correction for Lagrangian particle dispersion models. Boundary-Layer Meteorology 90, 155–167.

Stohl, A., Trickl, T., 1999. A textbook example of long-range transport: simultaneous observation of ozone maxima of stratospheric and North American origin in the free troposphere over Europe. Journal of Geophysical Research, in press.

Stohl, A., Wotawa, G., Seibert, P., Kromp-Kolb, H., 1995. Interpolation errors in wind fields as a function of spatial and temporal resolution and their impact on different types of kinematic trajectories. Journal of Applied Meteorology 34, 2149–2165.

Thomson, D.J., 1987. Criteria for the selection of stochastic models of particle trajectories in turbulent flows. Journal of Fluid Mechanics 180, 529–556.

Thorpe, A.J., 1997. Attribution and its application to mesoscale structure associated with tropopause folds. Quarterly Journal of the Royal Meteorological Society 123, 2377–2399.

Tremblay, J., Servranckx, R., 1993. Beryllium-7 as a tracer of stratospheric ozone: a case study. Journal of Radioanalytical and Nuclear Chemistry 172, 49–56.

Tsutsumi, Y., Igarashi, Y., Zaizen, Y., Makino, Y., 1998. Case studies of tropospheric ozone events observed at the summit of Mount Fuji. Journal of Geophysical Research 103, 16935–16951.

Van Haver, P., de Muer, D., Beekmann, M., Mancier, C., 1996. Climatology of tropopause folds at midlatitudes. Geophysical Research Letters 23, 1033–1036.

van Velthoven, P.F.J., Kelder, H., 1996. Estimates of stratosphere–troposphere exchange: sensitivity to model formulation and horizontal resolution. Journal of Geophysical Research 101, 1429–1434.

Vaughan, G., 1988. Stratosphere–troposphere exchange of ozone. In: Isaksen, I.S.A. (Ed.), Tropospheric Ozone. D. Reidel Publishing Company, Dordrecht, The Netherlands, pp. 125–135.

Vaughan, G., Price, J.D., Howells, A., 1994. Transport into the troposphere in a tropopause fold. Quarterly Journal of the Royal Meteorological Society 120, 1085–1103.

Volz, A., Kley, D., 1988. Evaluation of the Montsouris series of ozone measurements made in the nineteenth century. Nature 332, 240–242.

Wakamatsu, S., Uno, I., Ueda, H., Uehara, K., Tateishi, H., 1989. Observational study of stratospheric ozone intrusions into the lower troposphere. Atmospheric Environment 23, 1815–1826.

Waugh, D.W., 1996. Seasonal variation of isentropic transport out of the tropical stratosphere. Journal of Geophysical Research 101, 4007–4023.

Waugh, D.W., Plumb, R.A., 1994. Contour advection with surgery: a technique for investigating finescale structures in tracer transport. Journal of Atmospheric Science 51, 530–540.

Wei, M.-Y., 1987. A new formulation of the exchange of mass and trace constituents between the stratosphere and troposphere. Journal of Atmospheric Science 44, 3079–3086.

Weihs, P., Simic, S., Laube, W., Mikielewicz, W., Rengarajan, G., Mandl, M., 1999. Albedo influences on surface UV irradiance at the Sonnblick High Mountain Observatory (3106 m altitude). Journal of Applied Meteorology, in press.

Wernli, H., Davies, H.C., 1997. A Lagrangian-based analysis of extratropical cyclones. I: The method and some applications. Quarterly Journal of the Royal Meteorological Society 123, 467–489.

Wesely, M.L., 1989. Parameterization of surface resistances to gaseous dry deposition in regional-scale numerical models. Atmospheric Environment 23, 1293–1304.

Wirth, V., 1995. Comments on A new formulation of the exchange of mass and trace constituents between the stratosphere and troposphere. Journal of Atmospheric Science 52, 2491–2493.

Wirth, V., Appenzeller, C., Juckes, M., 1997. Signatures of induced vertical air motion accompanying quasi-horizontal roll-up of stratospheric intrusions. Monthly Weather Review 125, 2504–2519.

Wirth, V., Egger, J., 1999. Diagnosing extratropical synoptic-scale stratosphere–troposphere exchange: a case study. Quarterly Journal of the Royal Meteorological Society 126, 635–656.

Zanis, P., Schuepbach, E., Gäggeler, H.W., Hübener, S., 1999. Factors controlling Beryllium-7 at Jungfraujoch in Switzerland. Tellus, in press.